



HASP Student Payload Application for 2021

Payload Title: WANKA – A Mission to Measure Stratospheric Aerosols Parameters Using Low-Cost Commercial Sensors		
Institution: Universidad Nacional de Ingeniería		
Payload Class (Enter SMALL, or LARGE): SMALL		Submit Date: January 08, 2021
<p>Project Abstract: Interest in the study of stratospheric aerosols has increased due to their effects in the Earth’s radiative forcing. However, there is uncertainty about effects they cause, due to their high spatial and temporal variability, and physical and chemical processes to which they are exposed. This project develops a cost-effective way to measure some stratospheric aerosol properties: concentration and backscattering coefficient, which quantifies the radiation scattered in the opposite direction to that of incident radiation. Two measurement methods are going to be implemented: The first method uses a low-cost commercial Lidar (Class 1 laser), which lens will see outside the payload to calculate the aerosols backscattering coefficient. Second method will use low-cost commercial dust sensors to quantify aerosol concentration after an air heating process. The team is composed of students from different academic years and advised by an engineer from Geophysical Institute of Peru. Payload will weigh less than 3kg, its dimensions will be 15cm x 15 cm x 28.42 cm. It will require 12.34 Watts of power and a 5 bps downlink bandwidth.</p>		
Team Name: WANKA		Team or Project Website:
Student Leader Contact Information:		Non-Faculty Advisor Contact Information:
Name:	Ramiro Gustavo Tintaya Quispe	Luis Suarez-Salas
Department:	Mechatronic Engineering.	Sub Directorate of Atmospheric Sciences and Hydrosphere Geophysical Institute of Peru (IGP)
Mailing Address:	Av. San Miguel de Piura 213. Urb. San Juan de Dios. Jacobo Hunter.	Instituto Geofísico del Perú (IGP). Calle Badajoz 169. Urb. Mayorazgo, 4ta etapa – Ate.
City, State, Zip code:	Arequipa, Arequipa, Peru. ZIP code: 04011.	Lima, Lima, Peru. ZIP code: 15012.
e-mail:	rtintayaq@uni.pe	lsuarez@igp.gob.pe
Office Telephone:		
Mobile Telephone:	+51 954 154 873	+51 961 611 454

Flight Hazard Certification Checklist

NASA has identified several classes of material as hazardous to personnel and/or flight systems. This checklist identifies these documented risks. Applying flight groups are required to acknowledge if the payload will include any of the hazards included on the list below. Simply place an (x) in the appropriate field for each hazard classification. **Note:** Certain classifications are explicitly banned from HASP (grey filled items on table below) and the remaining hazards will require additional paperwork and certifications. If you intend to include one of the hazards, you must include detailed documentation in section 3.8 of the application as required by the HASP Call for Payloads.

This certification must be signed by both the team faculty advisor and the student team lead and included in your application immediately following the cover sheet form.

Hazardous Materials List		
Classification	Included on Payload	Not Included on Payload
RF transmitters		x
High Voltage		x
Pyrotechnics		X
Lasers (Class 3B or 4)		X
Intentionally Dropped Components		X
Liquid Chemicals		X
Cryogenic Materials		X
Radioactive Material		X
Pressure Vessels		X
Magnets		X
UV Light		X
Biological Samples		X
Li-ion Batteries		X
High intensity light source		X

Student Team Leader Signature:



Faculty Advisor Signature:



Table of Contents

Flight Hazard Certification Checklist	1
1. Payload Description	3
1.1 Payload Scientific / Technical Background	3
1.1.1 Mission Statement	3
1.1.2 Mission Background and Justification	4
1.1.3 Mission Objectives	5
1.2 Payload Systems and Principle of Operation	5
1.3 Major System Components	6
1.4 Mechanical and Structural Design	7
1.5 Electrical Design	11
1.6 Thermal Control Plan.....	22
1.6.1 Passive Thermal Control.....	22
1.6.2 Active Thermal Control	28
2. Team Structure and Management.....	30
2.1 Team Organization and Roles.....	30
2.2 Timeline and Milestones	34
2.3 Anticipated Participation in Integration and Launch operations	36
3. Payload Interface Specifications	36
3.1 Weight Budget.....	36
3.2 Power Budget	38
3.3 Downlink Serial Data	39
3.4 Uplink Serial Commanding	40
3.5 Analog Downlink	40
3.6 Discrete Commanding	40
3.7 Payload Location and Orientation Request.....	40
3.8 Special Requests.....	40
4. Preliminary Drawings and Diagrams.....	41
5. References	42
Appendix.....	44
Detailed mechanical drawings not required in previous sections	44
Detailed timeline and milestone WBS document	48
Detailed electrical drawings not required in previous sections	50
Preliminary PCB layout.....	52

1. Payload Description

The WANKA mission is a project developed by peruvian undergraduate students from the “Universidad Nacional de Ingeniería” and the “Pontificia Universidad Católica del Perú”, with the collaboration of engineers from the Geophysical Institute of Peru. Its main objective is the development of a payload capable of measuring optical and physical parameters of stratospheric aerosols.



Fig. 1. WANKA mission logo.

1.1 Payload Scientific / Technical Background

1.1.1 Mission Statement

The main objective of the WANKA mission is to develop a payload able to measure stratospheric aerosol parameters using low-cost commercial sensors. In order to achieve it, two methods of measurement are going to be implemented. First one is based on a low-cost commercial Lidar located in a way that its lenses can see outside the payload, intending to calculate the backscattering coefficient of stratospheric aerosols. Second method involves the measurement of stratospheric aerosol concentration using a low-cost commercial dust sensor. It will work after air is heated up to a temperature where the sensor works optimally. It is expected to fly on the 2021 HASP mission. And if it is successful, be a major step in the development of payloads for stratospheric aerosol parameters measurement designed and implemented by undergraduate students at an affordable cost.

1.1.2 Mission Background and Justification

During the last decade the interest in the study of stratospheric aerosols has increased, mainly due to their increase since 2000, and their potential applications to control global warming due to its negative effect on the Earth's radiative forcing. They are usually considered as the particles suspended in a gas, without a constant composition [1]. They affect the earth's radiative budget, absorbing and scattering the radiation that enters or leaves the planet. Working directly or indirectly, affecting the radiative properties and the lifetime of the clouds [2]. However, there is a lot of imprecision regarding the effect that they cause in the radiative forcing as it is shown in Fig. 2, where the aerosol parameters indicate high uncertainty. Stratospheric aerosols are found from the end of the tropopause up to a maximum height that depends on the sedimentation and evaporation process generated by the increase in temperature with the altitude, and are mainly composed by stratospheric sulfur from different gaseous molecules as sulfur dioxide (SO_2), carbonyl sulfide (OCS) and sulfuric acid (H_2SO_4), the ones that are produced mainly due to volcanic injections of SO_2 and aerosols. [1]

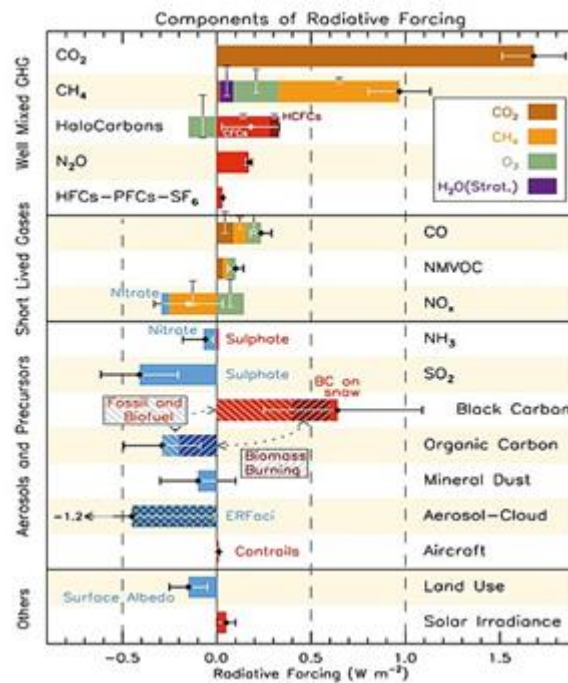


Fig. 2. Components of Earth's radiative forcing with their corresponding uncertainty (Source: Adapted from [3, Fig. 8.17]).

There are different ways to measure stratospheric aerosol parameters: in situ, ground based and space based. Space based missions use mainly satellites, as CALIPSO, which provides backscattering profiles assuming a static lidar ratio for all the latitudes and longitudes, or the SAGE missions that calculate backscattering coefficients using coefficient extinction and use data provided by ground-based systems to verify its algorithms. Ground based measurements use powerful lidar systems. There are many places in the world with this instrument, as Table Mauna Loa at USA or the "Observatoire de Haute-Provence" at France [4], and different instruments that can acquire this data as the Raman Lidar or Ceilometers [5]. One of the ceilometers used to measure these parameters is the CL31, which works at 905 nm, a wavelength where the molecular scattering is very weak, usually below the sensitivity of the instrument. [6]

In situ measurements are the most affordable way to measure stratospheric aerosol parameters, they can be sent to the stratosphere using balloons, and its payload can be composed by commercial sensors and actuators. They are not supposed to replace the other techniques, but can provide highly complementary information, and can be built by students from different academic years [7]. One of these missions is Compact Optical Backscatter Aerosol Detector (COBALD), which provides high precision measurements of optical parameters as the Backscattering coefficient at 455 nm and 940 nm, but cannot work during the day [5]. Another mission is developed by High-Altitude Balloon for Outreach and Research (HARBOR), which measures aerosol and gases concentration using low-cost commercial sensors [8].

1.1.3 Mission Objectives

The WANKA mission has two main scientific objectives:

- Measurement of stratospheric aerosol backscattering coefficient during the day and night using a low-cost commercial lidar. The data acquired will be compared with the data given by the Calipso satellite, to confirm its reliability.
- Measurement of stratospheric aerosol concentration using low-cost commercial dust sensors. The data acquired will be compared with the data obtained after processing the Calipso satellite measurements to obtain stratospheric aerosol concentration [9], in order to confirm the reliability of the data acquired by our mission.

1.2 Payload Systems and Principle of Operation

To monitor the stratospheric aerosol concentration, it is going to be implemented a system similar to [8], where a constant flow of external air is needed. To achieve this, the following closed air circuit has been designed. The incoming air will first be heated by the active heating system. It will then pass by the dust sensor GP2Y1010AU0F, which will measure the concentration of PM 2.5 particles, and the gas sensor MQ135, which will measure the gas composition. At last, it will arrive at the pumping system which consists of a rotary vane pump DC06/21FK and an air flow sensor AWM5101VN. This system will have a closed control loop in order to obtain a constant air flow. The air will first pass through the air flow sensor and finally be pumped out by the rotary vane pump.

The mission will also use a low-cost commercial LIDAR, with the advantage of making direct measurements in the stratosphere, instead of using powerful Lidar. The laser beam that Lidar will emit will be scattered by stratospheric aerosols since the Lidar emits waves of 905 nm, the same wavelength as the CL31 ceilometer, knowing and applying the post-processing equations of the data, we will be able to know properties such as stratospheric aerosol backscattering coefficient.

1.3 Major System Components

WANKA is composed of two major subsystems, the ones that will measure the backscattering coefficient and the concentration of the aerosols. Two additional subsystems will be considered, a system to transmit the critical parameters by telemetry and to save data in a micro-SD module and a system to acquire GPS data. The payload will acquire GPS data using a commercial module, to acquire this data independently, but also it will receive it from HASP, to ensure correct data acquisition during the flight, and to verify that the data acquired by the module within the payload is correct.

1.3.1. Lidar system

- a. Components: Lidar Lite V3, Heating Pad, SHT31 temperature and humidity sensor.
- b. Purpose: Measurement of stratospheric aerosol backscattering coefficient applying the elastic-backscatter single-scattering lidar equation. [10]
- c. Resource: The Lidar and the sensors run on 5V and the heating pad will work using an analog voltage from 0V to 5V. The system consumes 3.678 W considering the heating pad.
- d. Description: Lidar will be embedded in the layer of rigid polyurethane foam, in order to keep its internal circuits at a suitable temperature. The heating pads will be activated if the temperature drops below the minimum operating temperature of the lidar according to the active thermal control plan. The lenses point outwards and will be exposed to low temperatures from the stratosphere, but there is no need to coat them with a thermal protector since the fatigue produced by low temperatures (near to -70°C) is negligible in the dimensions of these lenses, furthermore, a thermal protector might interfere with the emitted and received beam. [11]

1.3.2. Aerosol concentration sensor system

- a. Components: GP2Y1010AU0F Dust Sensor, two heating pads, SHT31 temperature and humidity sensor, MQ135 gas sensor, AWM5000 flow sensor.
- b. Purpose: Measurement of stratospheric aerosol concentration at different heights and places.
- c. Resource: Flow sensor runs on 10V, the rest of the sensors runs on 5V and the heating pad uses an analog voltage from 0V to 5V. The whole system consumes 8.34W considering the two heating pads.
- d. Description: This system will measure the concentration of stratospheric aerosols using low-cost commercial dust sensors. In order to achieve a temperature where sensors can work, external air will be absorbed and heated using two heating pads, to absorb the air it will be used a vacuum suction pump, and a flow sensor will be used to know if the pump is working and optimize its power consumption. All these components will be located inside an aluminum box that has two holes to let the absorbed air pass.

1.3.3. GPS data acquisition system

- a. Components: GPS NEO-6M module (includes receiver and antenna)
- b. Purpose: Acquire latitude, longitude, altitude and time data.
- c. Resource: GPS NEO-6M module runs on 5V and consumes 185 mW.
- d. Description: This system will acquire latitude, longitude and altitude to generate a full profile of the aerosol parameters after the flight, and also a timestamp to include it on in the data. The GPS antenna will be located above the payload, partially embedded in the

layer of rigid polyurethane foam to improve the data acquisition. The GPS receiver will be inside the same box as the aerosol concentration sensor system.

1.3.4. Data management system

- a. Components: SparkFun Transceiver Breakout RS232, microSD card reader module.
- b. Purpose: The data transmission system will convert serial data from TTL to RS232 to send it by telemetry and also save it in a microSD module.
- c. Resource: Sparkfun Transceiver and microSD card runs on 5V. The system consume 1.2W.
- d. Description: This system is located inside the same box as the aerosol concentration sensor system. It will send data by telemetry and save it in the micro-SD card sequentially.

1.4 Mechanical and Structural Design

The main structure is based on a geometry that resembles a parallelepiped of 15 cm deep, 15 cm wide, and 28.4cm high. The structure is covered by aluminum sheets on the side faces and thermal insulation made of Polyurethane foam on the inside, the structure also contains a removable bottom face and the top face which are assembled to the body by bolts allowing easy access to the electronic sub-modules.

Due to its high hardness and low density, Aluminum 7075 was chosen as the structural material. In order to ensure that the payload remains intact and attached to the mounting plate, a 10 g vertical and 5 g horizontal shock was applied over a finite element simulation in the commercial software Ansys Structural.

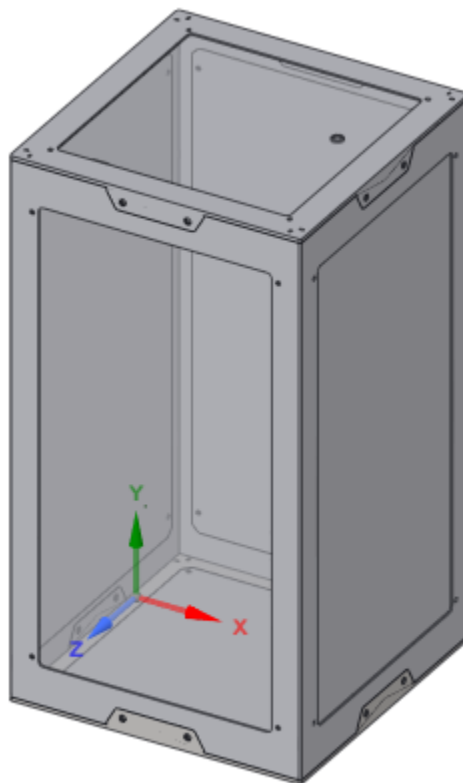


Fig. 3. Structural Design.

In Fig. 4 it can be seen the total deformation, Fig 5. shows the stresses under which the payload will be and Fig 6. shows the safety factor product of these loads.

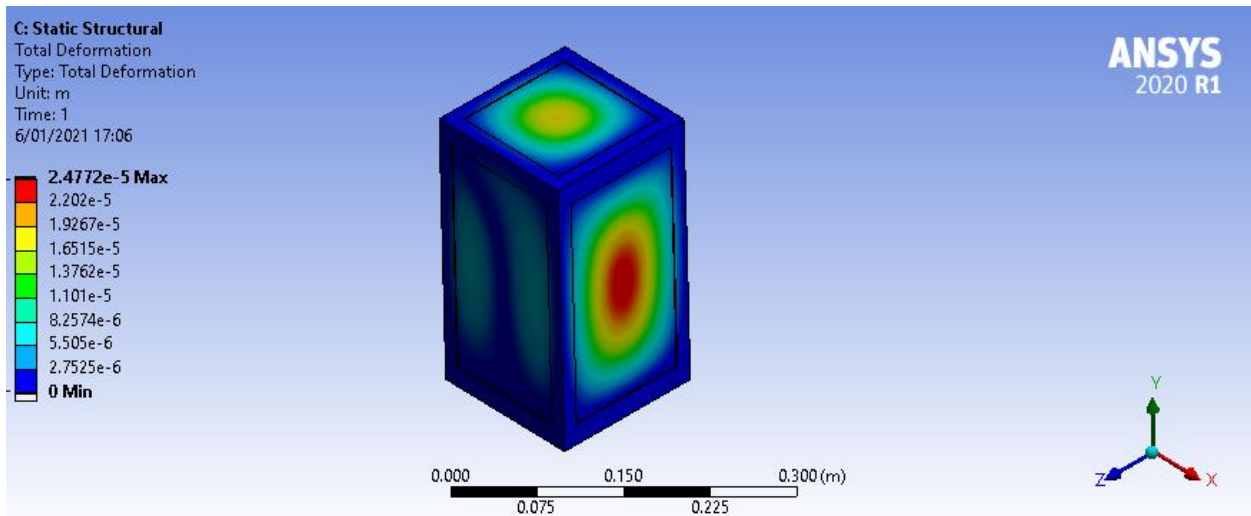


Fig. 4. Total deformation under a 10 g vertical and 5 g horizontal shock.

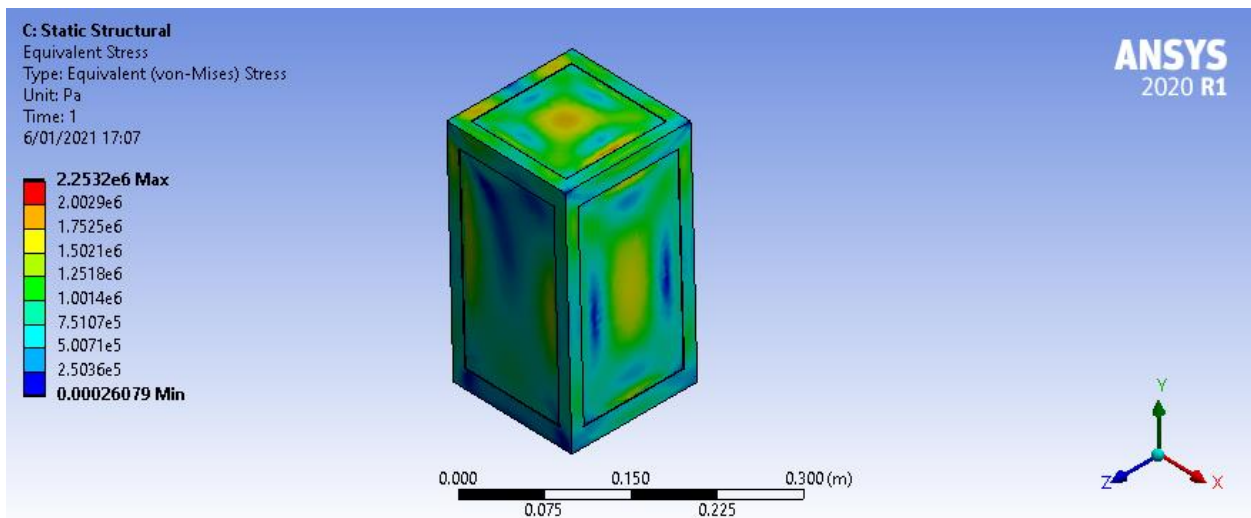


Fig. 5. Stress over the mechanical structure under a 10 g vertical and 5 g horizontal shock.

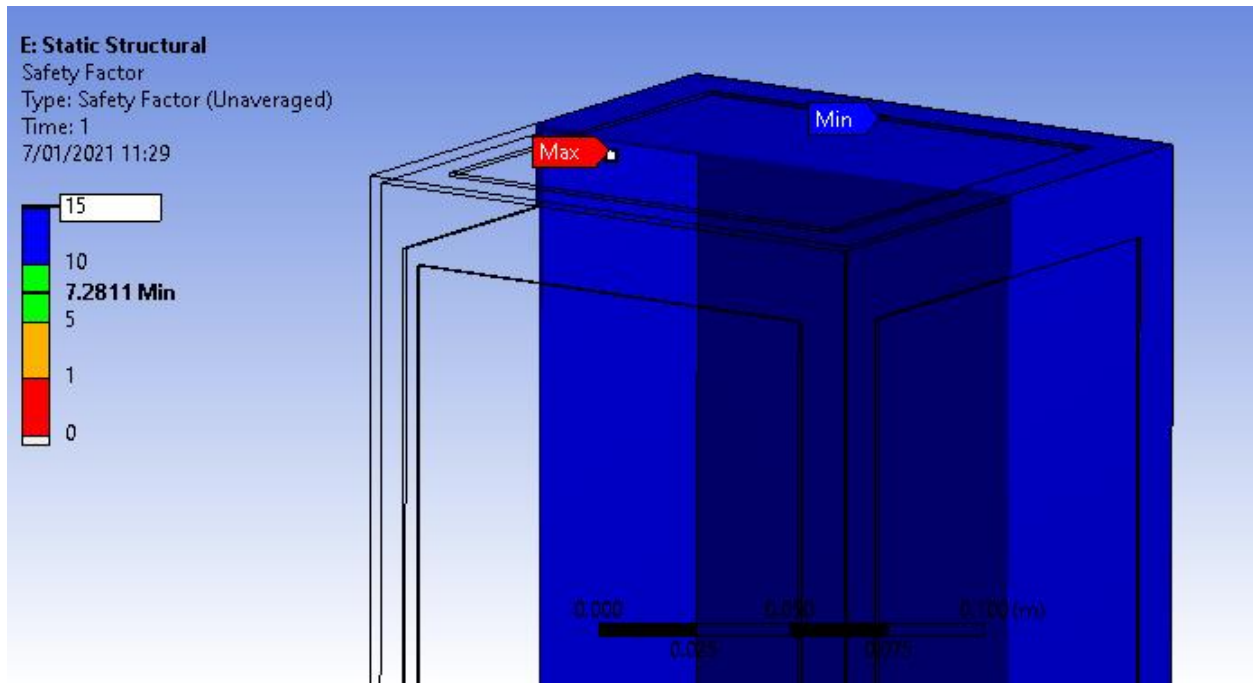


Fig. 6. Safety factor under a 10 g vertical and 5 g horizontal shock.

A minimum safety factor of 7.28 will guarantee that the structural design and its material chosen will remain intact and attach to the mounting plate.

Fig 7 shows how the payload will be attached to the payload mounting plate. As shown in Fig. 7 rivet nuts will join the payload and the payload mounting plate. In Fig 8 a detail of the fastening cross-section is shown.

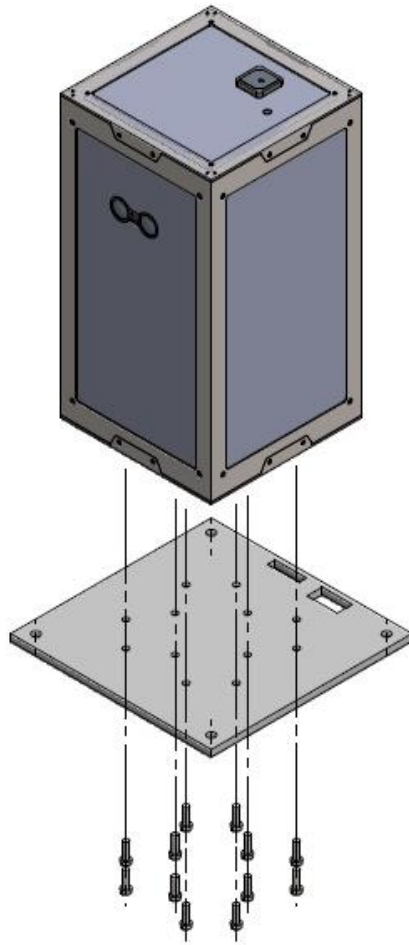


Fig. 7. Payload mounting plate interface.

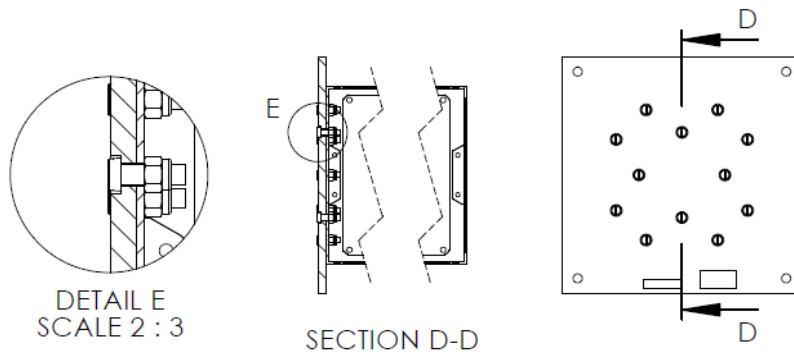


Fig. 8. Fastener cross section.

The detailed planes of the structural design and the modified mounting payload plate can be found in the appendix.

1.4.1. Magnetic protection

Electric arcs are electrons that move due to the existence of an electric field. These phenomena appear between two electrodes subjected to a voltage difference within a gaseous medium in which electrons can move through the field more easily. To cope with this phenomenon is necessary to make the electric field disappear, which will be done using the aluminum 7075 structure as a Faraday cage. Within this Faraday cage, the electric field will be zero and this will allow the electrons to move in the circuit board. This solution is given because the data will be transmitted using cables and we will not use a RF transmitter.

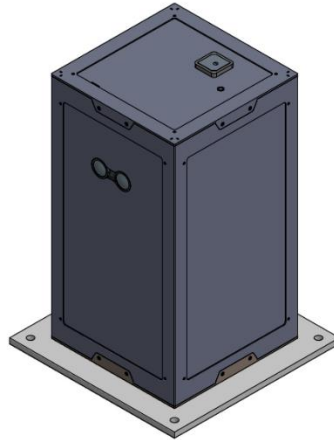


Fig. 9. Isometric view of the payload attached to the plate interface.

1.5 Electrical Design

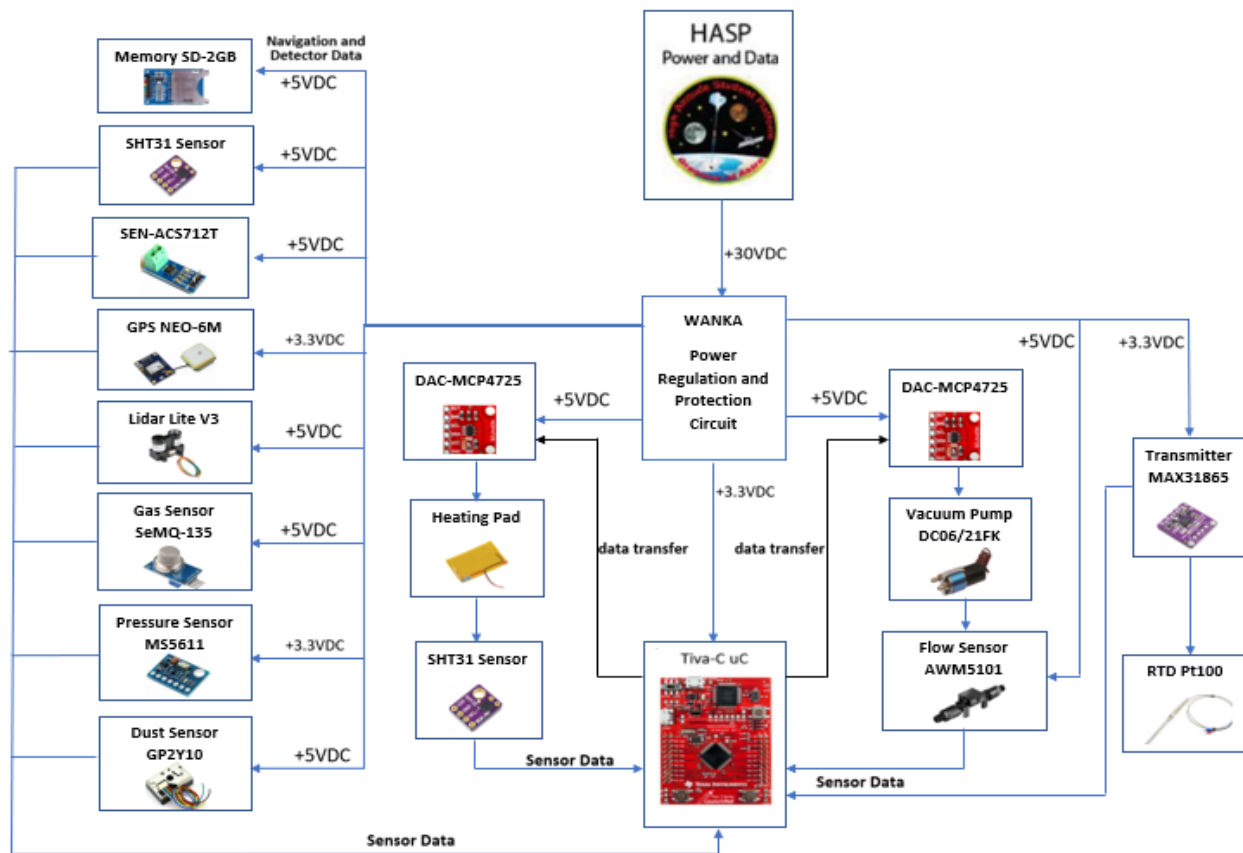


Fig. 10. Preliminary WANKA schematic.

Temperature and relative humidity sensor:

The temperature and humidity inside the payload will be measured with two SHT31 sensors, one of them will be used as a reference to determine the amount power to deliver by the heating pads and the other will allow us to know the temperature and humidity changes inside the payload. Using this data, we will be able to determine when to shut down non-critical systems to avoid damaging the circuit. The SHT31 sensor will be connected to two power cables and two I2C data cables.



Fig. 11. SHT31 temperature and relative humidity sensor.

RTD temperature sensor:

A RTD Pt100 sensor will be used to measure the temperature outside the payload, due to its optimal operation at low temperatures, its high precision and the linear relationship between its internal resistance and the external temperature. The three-wire model was chosen because it decreases the error generated by the wires.

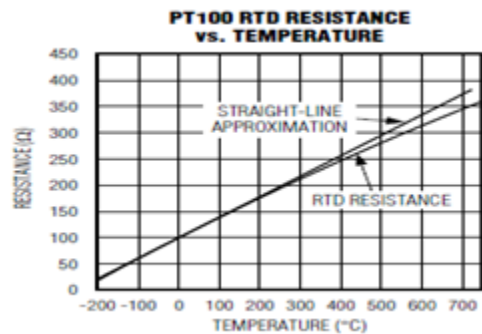


Fig. 12. RTD PT100 Temperature Sensor (3-wire) and output curve.

RTD transmitter:

The MAX31865 transmitter allows us to obtain the temperature measurements of the RTD Pt100 sensors reliably and easily. The module is responsible for reading the resistance of the Pt100 sensor and converting this analog signal into digital data to be interpreted by the Tiva-C microcontroller, this data will allow us to compare the actual measured with those expected in our simulation.



Fig. 13. MAX31865 transmitter module.

Pressure Sensor

As the payload ascends, the atmospheric pressure will constantly decrease, to measure these variations we will use the MS5611 sensor which takes high precision measurements with a low energy consumption. This sensor will also indicate when to shut down non-critical systems to avoid damaging the circuit.



Fig. 14. MS5611 Pressure Sensor.

GPS Module

The GPS NEO-6M will allow us to locate the payload during the whole flight, this module was chosen due to its high performance, low power consumption, high sensitivity (165 dBm), and frequency of update of 5Hz. It is connected to the micro controller through serial protocol.



Fig. 15. NEO-6M GPS Module.

Current sensor

It is necessary to control the current delivered by the PBY10 converters, since we are connecting several devices to a single source. The ACS712T sensor will be used to achieve it. This sensor allows the measurement of AC or DC current in the range of 0 to 20 amperes.

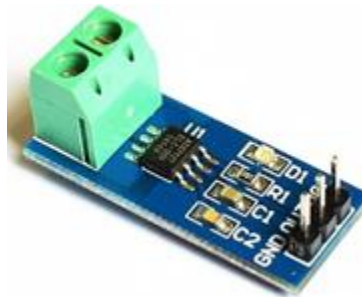


Fig. 16. ACS712T-20A Current Sensor.

Dust Sensor

Regarding the measurement of the concentration of PM 2.5 particles, the Sharp GP2Y1010AU0F Dust sensor was chosen. It retains a linear relationship between the output voltage and dust sensor density between 0 and 0.5 mg/m³, which falls within our expected dust density values. The analog values obtained will be converted to digital values through the ADC module of the Tiva-C microcontroller.

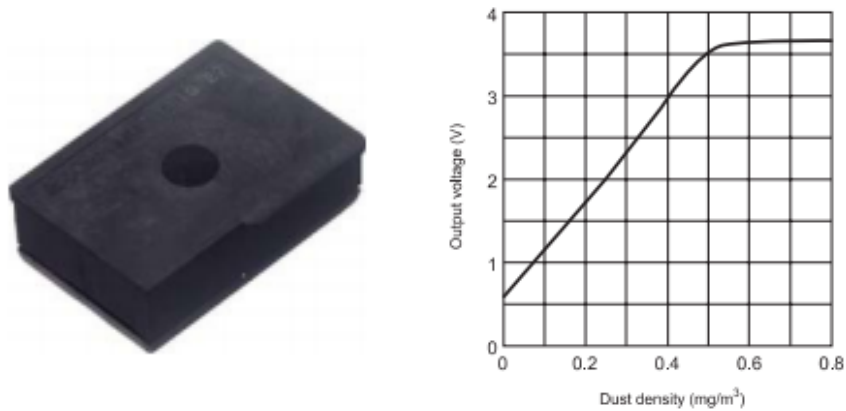


Fig. 17. Sharp GP2Y1010AU0F Dust Sensor and Output curve.

Gas Sensor

For this study it is indispensable to know the composition of the measured air. For this purpose, we selected the SEN-MQ135 gas sensor which is commonly used in air quality control equipment for buildings and offices. Internally, this sensor heats the air that passes through it and measures the conductivity of that air. Which is why it is suitable for detecting NH₃, NO_x, alcohol, Benzene, smoke, CO₂ and a variety of other pollutants. Depending on the pollutant chosen it will have a different sensitivity as shown on Fig. 18.

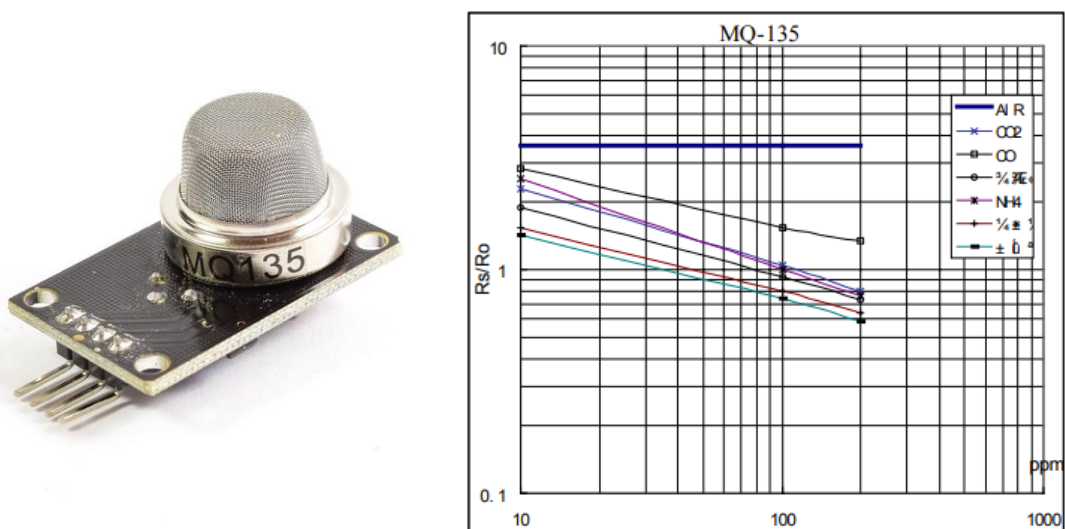


Fig. 18. MQ135 Gas Sensor and Sensitivity Curve for Different Gases.

Rotary Vane Pump

Concerning the method by which to increase the normal air flux and maintain a regular flux, a rotary vane pump was chosen. It consists of vanes mounted to a rotor that rotates inside a cavity, those vanes maintain contact with the walls in order to displace the fluid contained within as shown in Fig. 19. For this application, the DC06/21FK model from Fürgüt was selected.

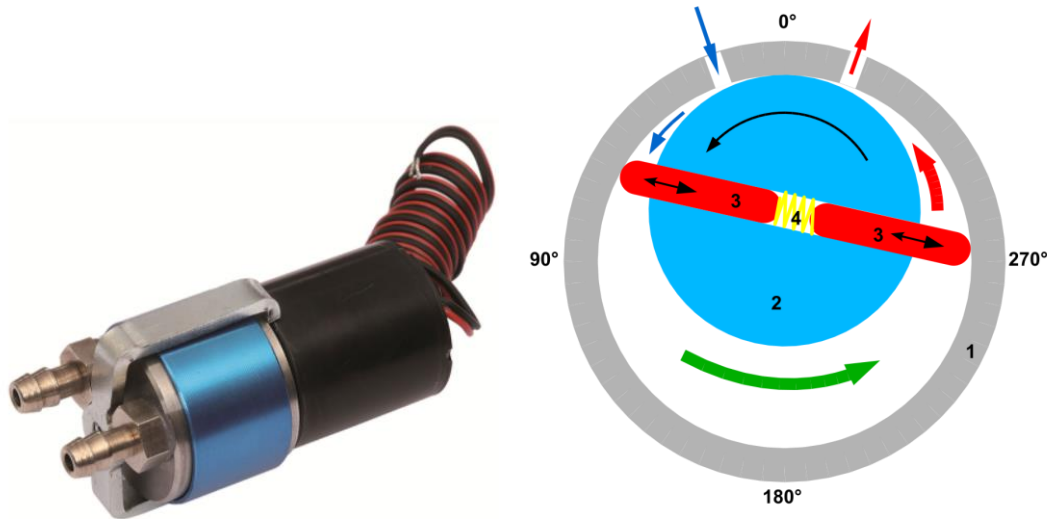


Fig. 19. DC06/21FK Motor with a diagram explaining its operation.

This motor will be powered by the DAC MCP4725 module which will vary its energy output data according to the schematic shown in Fig. 10.

Flow Sensor

In order to measure the inlet airflow across the pipes, we considered from Honeywell the AWM5000 Series flow sensors which can make in-line measurements and is conditioned with a linearization circuit to have a linear relationship between voltage and flow as shown below.

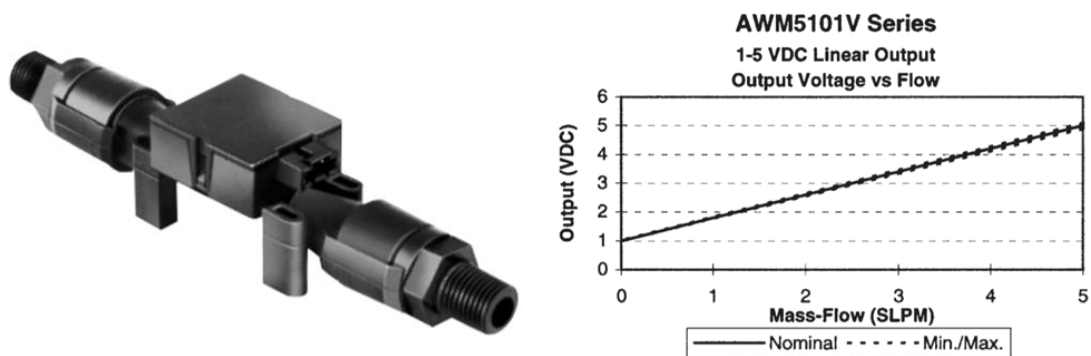


Fig. 20. WM5000 Series Sensor and Output Curves.

According to the vacuum pump working range, from this Series, we selected the AWM5101VN sensor which has a flow range of 0 to 5 SLPM and is calibrated for Air and N₂ flow measurements. Finally, the output analog voltage obtained is converted to digital values with the ADC module of the Tiva-C microcontroller.

Heating Actuator

Considering an Active Thermal Control, we selected a 5x15cm Heating Pad which works from 0-5 VDC and can elevate the surrounding ambient temperature to 60°C. The fact that these Heating Pads are low power (3W) makes them ideal for this application. Finally, in order to control this actuator with the Microcontroller, it is necessary to use the MPC4725 DAC transducer as shown in the electric diagram.

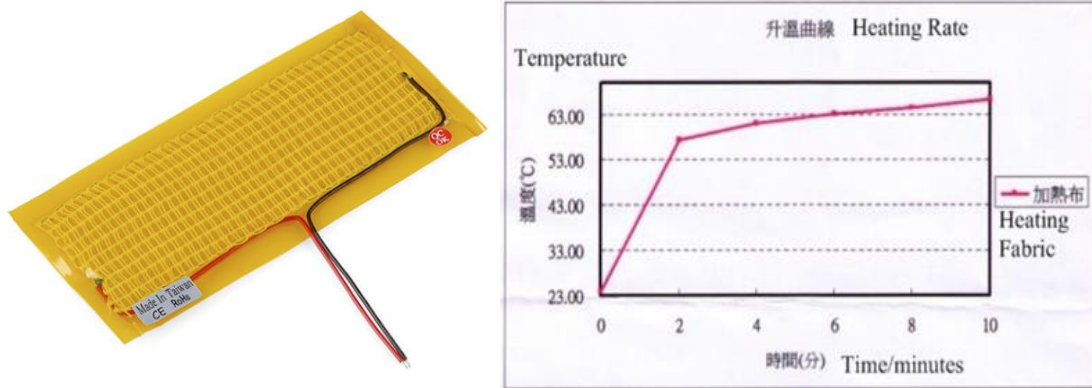


Fig. 21. Heating Pad and WarmUp Profile.

RS232 Transceiver

Following the HASP documentation, we handle the problem of TTL/RS232 levels interface with the use of the SparkFun Transceiver Breakout RS232 which has a maximum bit rate of 250 kbps (bits per second). This transceiver works well with 3.3V or 5V voltage sources.



Fig. 22. SparkFun Transceiver Breakout RS232.

Microcontroller

Tiva Launchpad will be used to control the system, it uses the TM4C123GH6PM microcontroller from Texas Instruments, as it has advantages over the Arduino, also available in our local market. One of these advantages is that it is a 32-bit microcontroller as opposed to the 8-bit ATMEGA 328P used by the Arduino Uno, and it also has more connectivity since it has 8 UART ports, 4 I2C modules, and more analog ports.

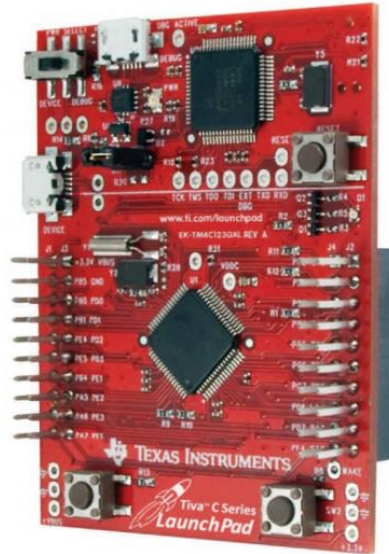


Fig. 23. TM4C123GXL - LAUNCHPAD Tiva C.

A comparative chart is presented in Table 1.

Table 1. Comparative chart.

	TM4C123GH6PM	ATMEGA328P
Power Supply	3.3V / 17.6 mA at 25°C operating at 16Mhz	5V/14 mA at 25°C operating at 16Mhz
I2C Ports	6	1
Universal Asynchronous Receivers Transmitters (UART)	8	1
Serial Peripheral Interface (SPI)	4	1
Analog to Digital Converter (ADC)	2	6
Operating Range (Ambient)	-40°C to 105°C	-55°C to 125 °C

LIDAR

The LIDAR model to be used is the LIDAR-Lite v3 from the company GARMIN, which emits a class 1 laser with a peak power of 1.3W with a wavelength of 905nm. It will be powered with 5v and it consumes 135mA in operation. [12]



Fig. 24. LIDAR-Lite v3.

PBY10 DC-DC converter

Two PYB10 converters will be used to distribute the energy, as each one can transfer up to 8W. These converters will be connected to the EDAC port using a protection against overcurrent (fuse). They will set the input voltages from 30 V to 5 V to supply the electronic components. Its main features are:

- Input voltage: 9V -36V
- Number of Outputs: 1 - 2
- Output Voltage: 3.3V, 5V, 12V, 15V, 24V.
- Maximum Output Power: 8W
- Operating Temperature: -40°C ~ 85°C



Fig. 25. PBY10 DC-DC converter.

LM1117 regulator

LM1117 regulator is used to set a voltage from 5V to 3.3V to supply some electronic components. It has a maximum output current of 1A, and operates down to a 1V dropout.

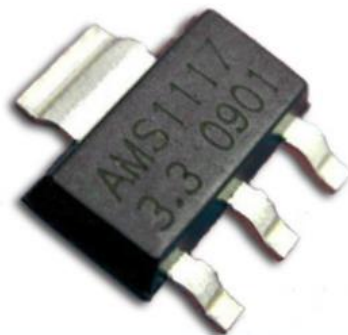


Fig. 26. LM1117 regulator.

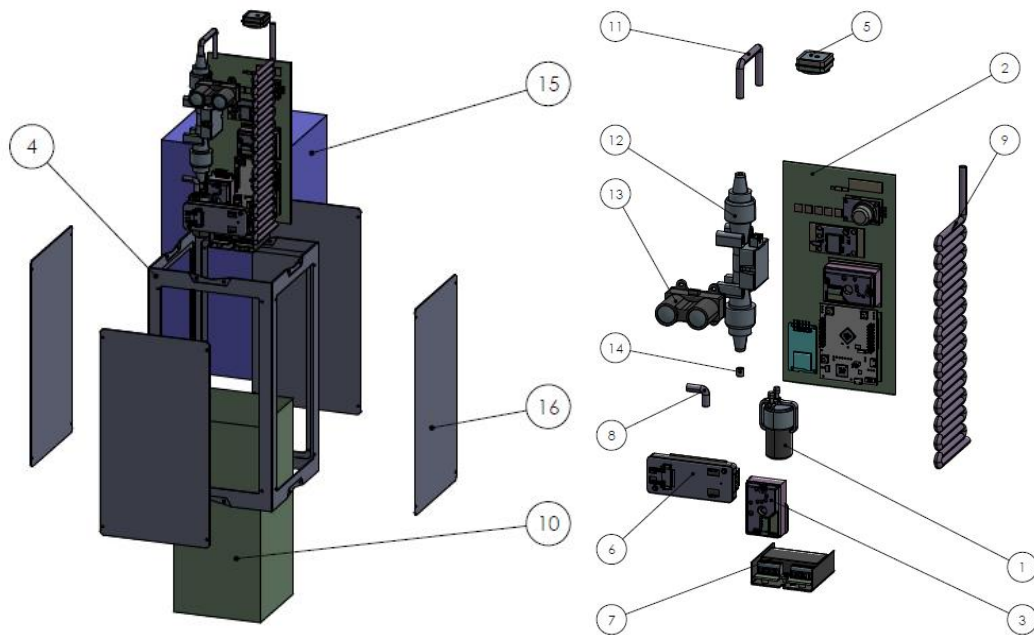


Fig. 27. Exploded view of structural and electronic components.

Table 2. Components of the general assembly.

N.º OF ELEMENT	PIECE N.º	QUANTITY
1	VACUUM PUMP	1
2	PCB ASSEMBLY	1
3	SENSOR GP2Y10	1
4	ARMOUR	1
5	ANTENNA	1
6	CUI PYB10-Q24-S12-DIN	1
7	PYB10-Q24-S5-U	1
8	COUPLING PIPE	1
9	SERPENTIN	1
10	ALUMINUM COATING	1
11	COUPLE 1	1
12	airflow sensor	1
13	LIDAR V3	1
14	COUPLE 2	1
15	THERMAL INSULATOR	1
16	ALUMINUM SHEETS	4

1.6 Thermal Control Plan

As per reference of the 2006 HASP flight, Fig. 28 shows the temperature variation during the whole flight. The red curve is from a sensor placed in the location of a large payload and the blue curve, which is of our interest, is the temperature at a small payload. The depth at the small payload curve occurs at about 17:00 and is due to passage through the tropopause, then the temperature will warm once float altitude is reached. After sunset, at about 2:00 UTC the temperature will drop again to very low values. Due to this large temperature range condition, a passive and active thermal control plant was implemented over the payload in order to ensure that all the internal components work correctly.

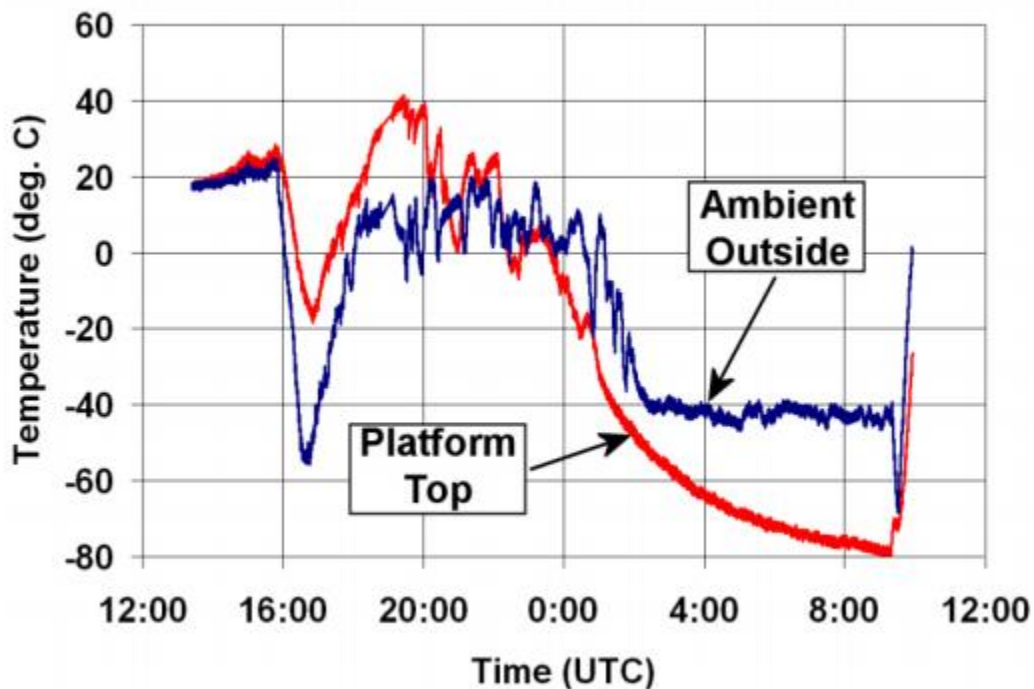


Fig. 28. Typical temperature during flight. (Source: HASP 2021 CFP)

1.6.1 Passive Thermal Control

The payload systems used are sensitive to low temperatures, being $-10\text{ }^{\circ}\text{C}$ the minimum temperature for the correct operation of the critical components of the circuit and $65\text{ }^{\circ}\text{C}$ the maximum temperature for the component with the lowest resistance. However, as it was previously established, the environment surrounding the payload has extreme conditions reaching very low temperatures that range from $-70\text{ }^{\circ}\text{C}$ to $24\text{ }^{\circ}\text{C}$ in all its trajectory which makes necessary the implementation of passive thermal control.

The passive thermal control implemented over the payload consists of rigid polyurethane foam of 20 mm of thickness. Polyurethane foam has a high thermal insulation capacity, which is not achieved with any other known material. It also has great resistance to solvents, aging, fuels, dissolved acids and alkalis, and the most aggressive industrial atmosphere.

In this manner, the payload will be insulated from within with the polyurethane foam with the objective to maintain a temperature range of $-10\text{ }^{\circ}\text{C}$ to $65\text{ }^{\circ}\text{C}$. In order to validate the thickness of the chosen material, a numerical simulation of fluid-solid coupling heat transfer of the payload was realized. A system coupling heat transfer simulation offers us a detailed fluid-structure interaction that will be advantageous to validate the passive thermal control.

Fig. 29 shows the general system coupling layout in Ansys Workbench, starting from Ansys Spaceclaim in which a simplified geometry of the payload structure, insulating material, and electronics components are drawn.

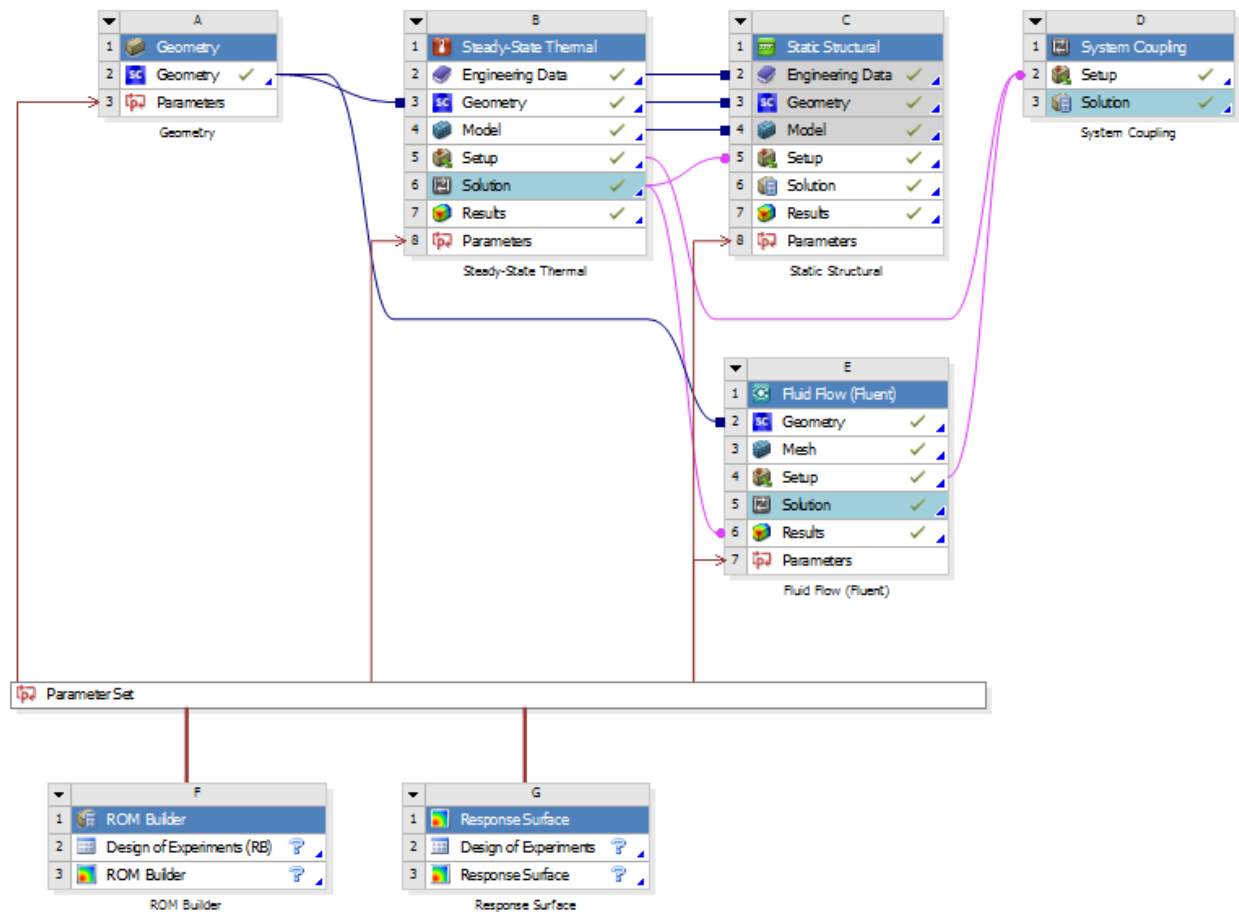


Fig. 29. General system coupling layout in Ansys Workbench.

Fig. 30 shows the simplified geometry, the structure geometry and insulating will be used for a thermal simulation while the electronic component's geometry will be used for the fluid simulation.

As stated, over the simplified geometry of the payload structure and insulating material a steady-state thermal simulation was performed in order to obtain a detailed temperature distribution over these solid materials.

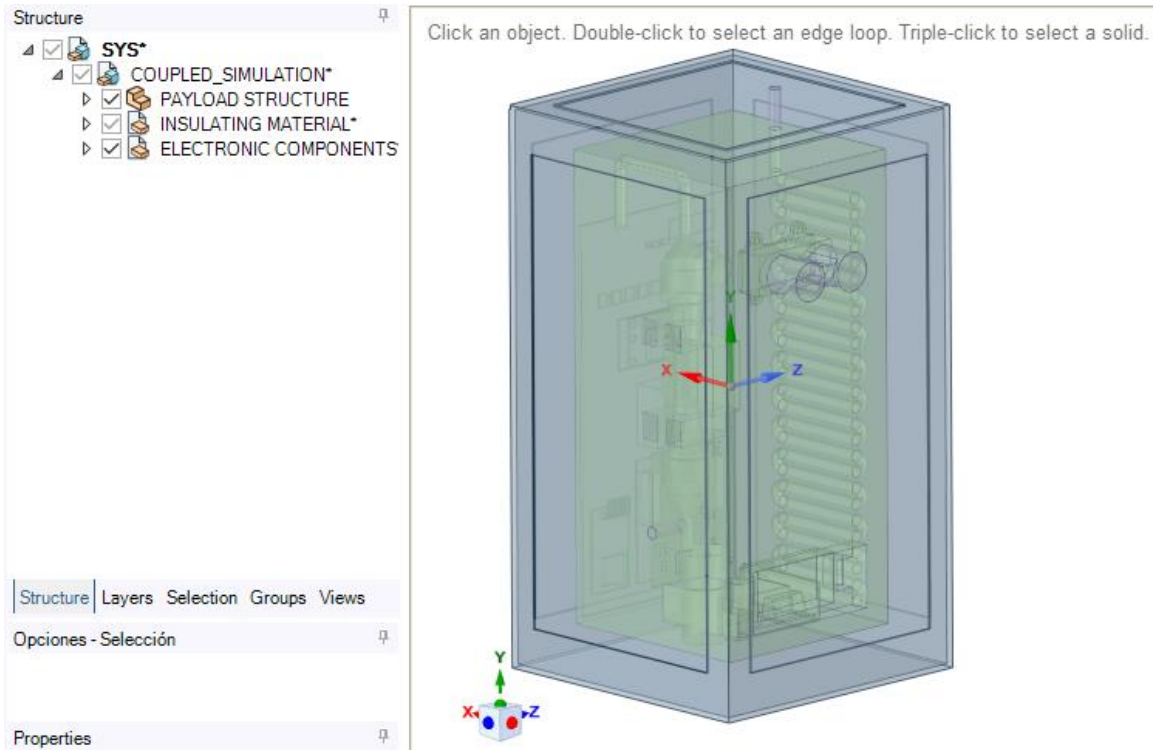


Fig. 30. Simplified geometry of the payload structure, insulating material and electronic components.

Fig. 31 and Fig. 32 show the temperature distribution over these structures and insulating geometry for the maximum and minimum temperature load which the payload will be put under.

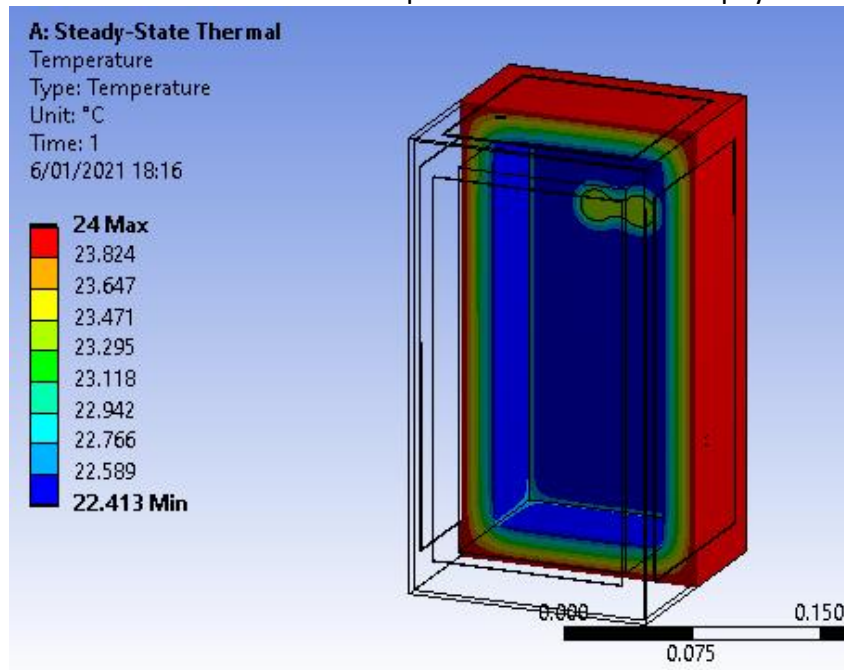


Fig. 31 Temperature distribution over the structure and insulating material geometry at 24 °C external temperature.

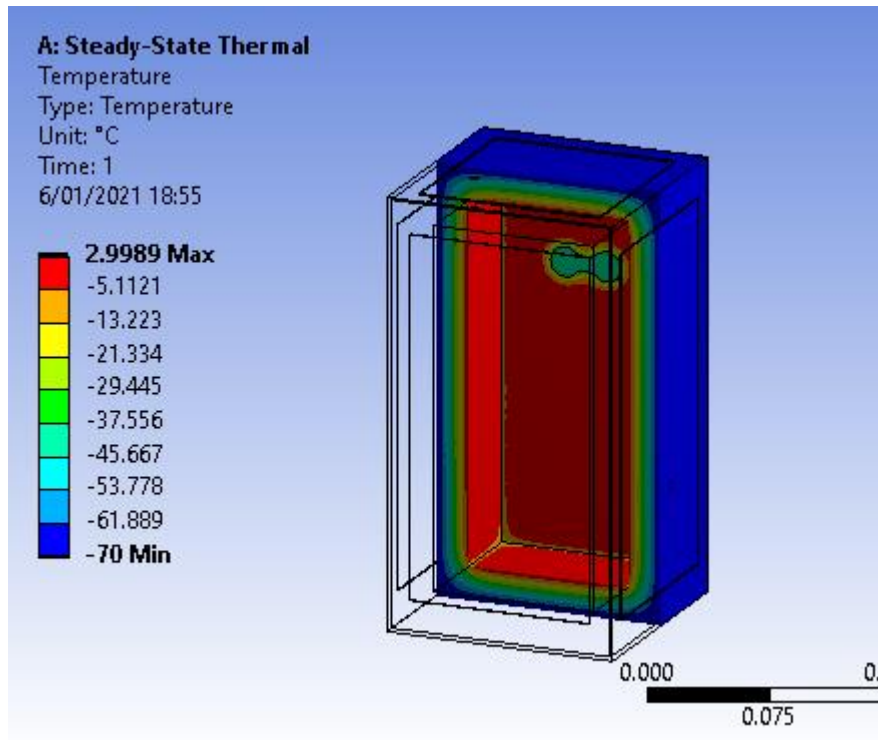


Fig. 32 Temperature distribution over the structure and insulating material geometry at -70 °C external temperature.

These temperature profiles from within the insulating material will be exported and used for an iterative coupled analysis between Ansys steady-state thermal and Ansys Fluent until certain criteria of convergence are achieved.

Fig. 33 and Fig 34 show the temperature distribution over the electronic component's geometry for the maximum and minimum temperature load which the payload will be put under.

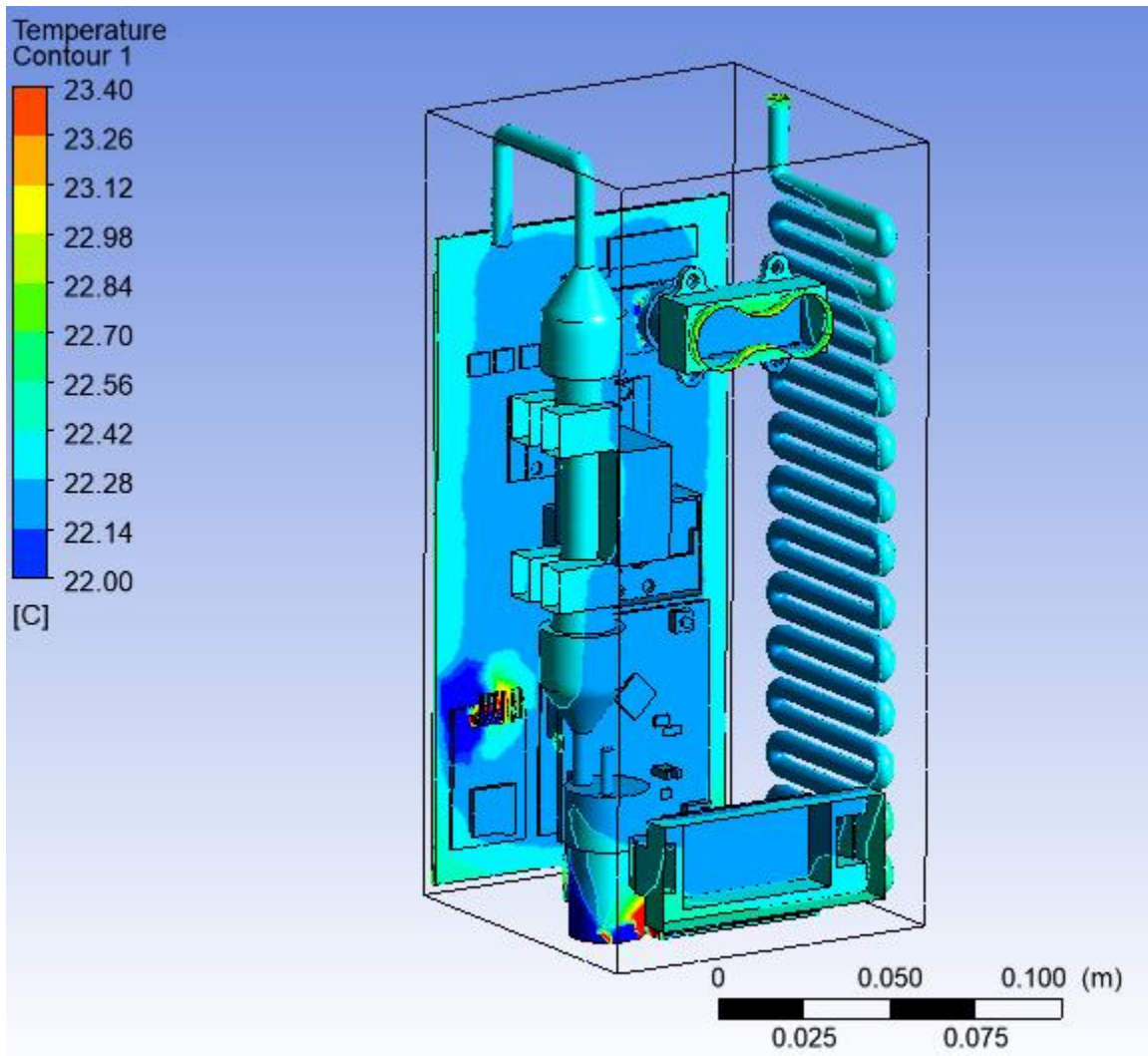


Fig. 33. Temperature distribution over the electronic component's geometry at 24 °C external temperature.

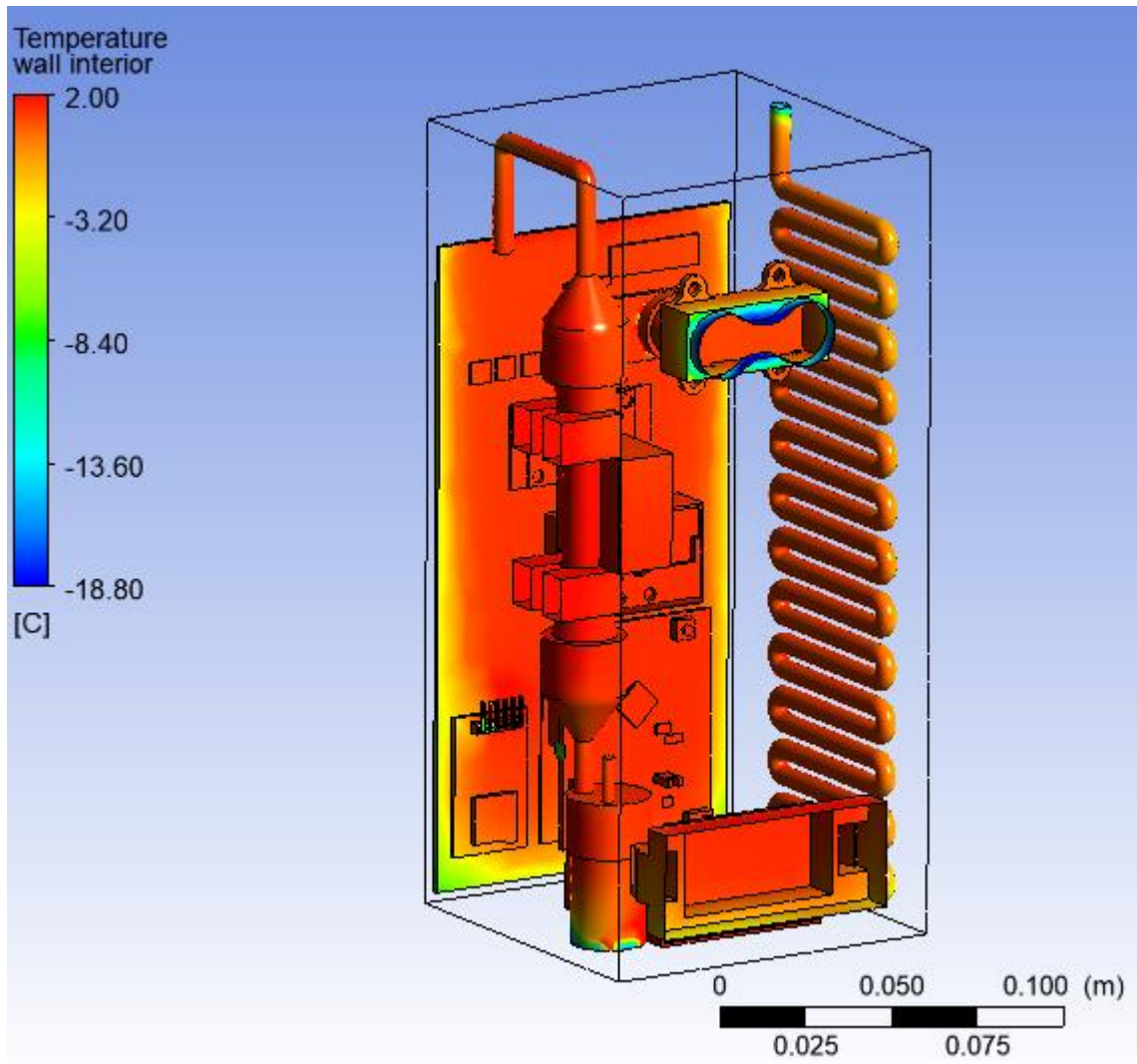


Fig. 34. Temperature distribution over the electronic component's geometry at -70°C external temperature.

With these results, we can guarantee a temperature range over the electronic components from 2°C to 23.4°C

Additionally, the electronic components have a passive thermal fin cooling system. There is a forced airflow that is used to improve the convection by the thermal fins. These fins function as a passive heat exchanger that transfers heat generated by an electronic device into the air, dissipating it away from the device, allowing the temperature of the device to be regulated.

1.6.2 Active Thermal Control

Even though the thermal simulation shows an acceptable range of temperature distribution for the electrical component's geometry, an active thermal control will be implemented as a contingency plan for any mishap (i.e., leaks) that can alter the temperature within the insulating material.

So, in order to avoid these harsh low temperatures (lowest values at 70°C) in critical components (i.e., LIDAR sensor, hose circuit) in case of any leaks, according to the temperature sensor's data, a heating pad (5V and 3W) will be used to regulate the temperature on these components. As this may cause the overall power consumption to exceed the HASP "Small payloads" limitations, a control strategy will be used to regulate the voltage of the heating pad according to the temperature and the current consumption. Moreover, to avoid the use of multiple heating pads, critical components will be positioned near only one.

The control strategy proposed is an intelligent PD controller shown in Fig. 35, which is a Model-Free Control algorithm used when the mathematical dynamic model of the system is not well known (i.e., the temperature dynamic model during the ascend of the Stratospheric Balloon).

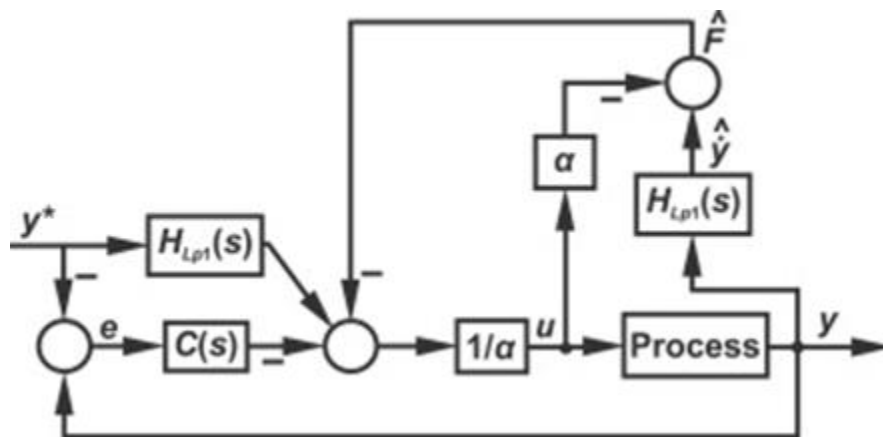


Fig. 35. iPD Control System [13].

Finally, as this control algorithm will be implemented in the TIVA-C microcontroller, it will be necessary the use of a DAC transducer. The one selected is the MPC4725 which has the characteristics shown below:

Table 3. MPC4725 characteristics.

Model	Voltage Input	Bit Resolution	Temperature Cond.	Communication
MPC4725	2.7V to 5.5V	12 Bits	-40 to 125 °C	I2C Interface

Thus, the circuit diagram of the whole control system is shown in Figure 36.

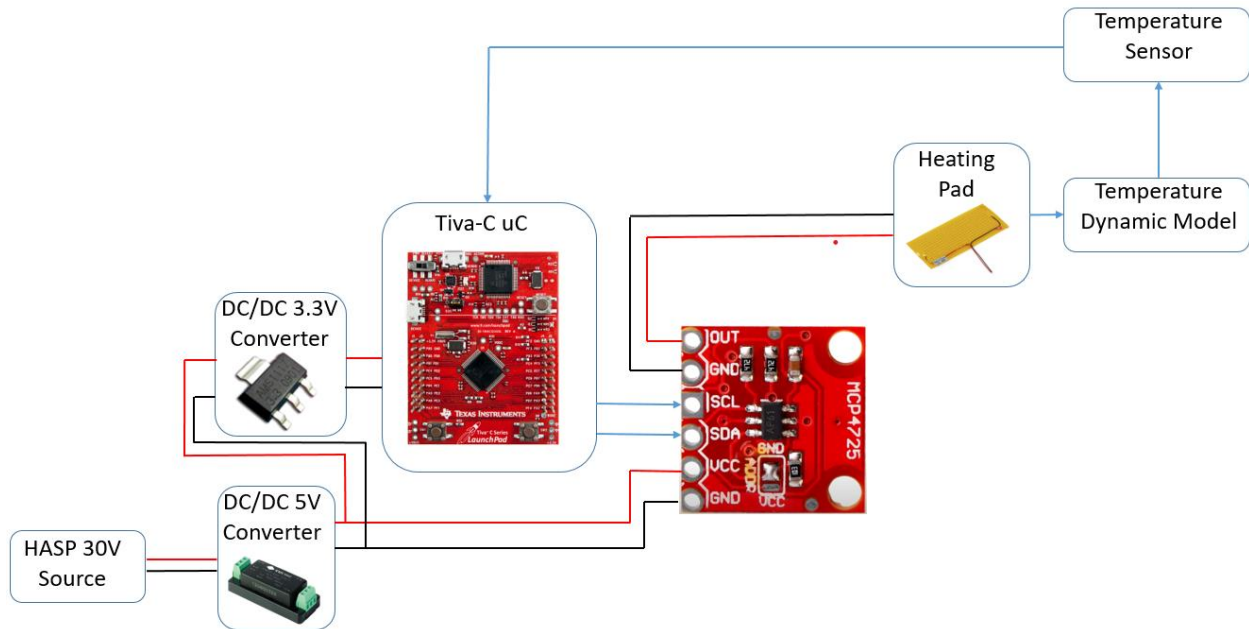


Fig. 36. Control System's Circuit Diagram.

Fig. 37 shows the temperature distribution on the electronic component's geometry taking into consideration the 2 heating pads on the critical components which are the Lidar sensor and the hose air circuit for the most critical temperature of -70 °C.

As we can see, a fully functional heating pad can increase the interior temperature of the payload by 8°C.

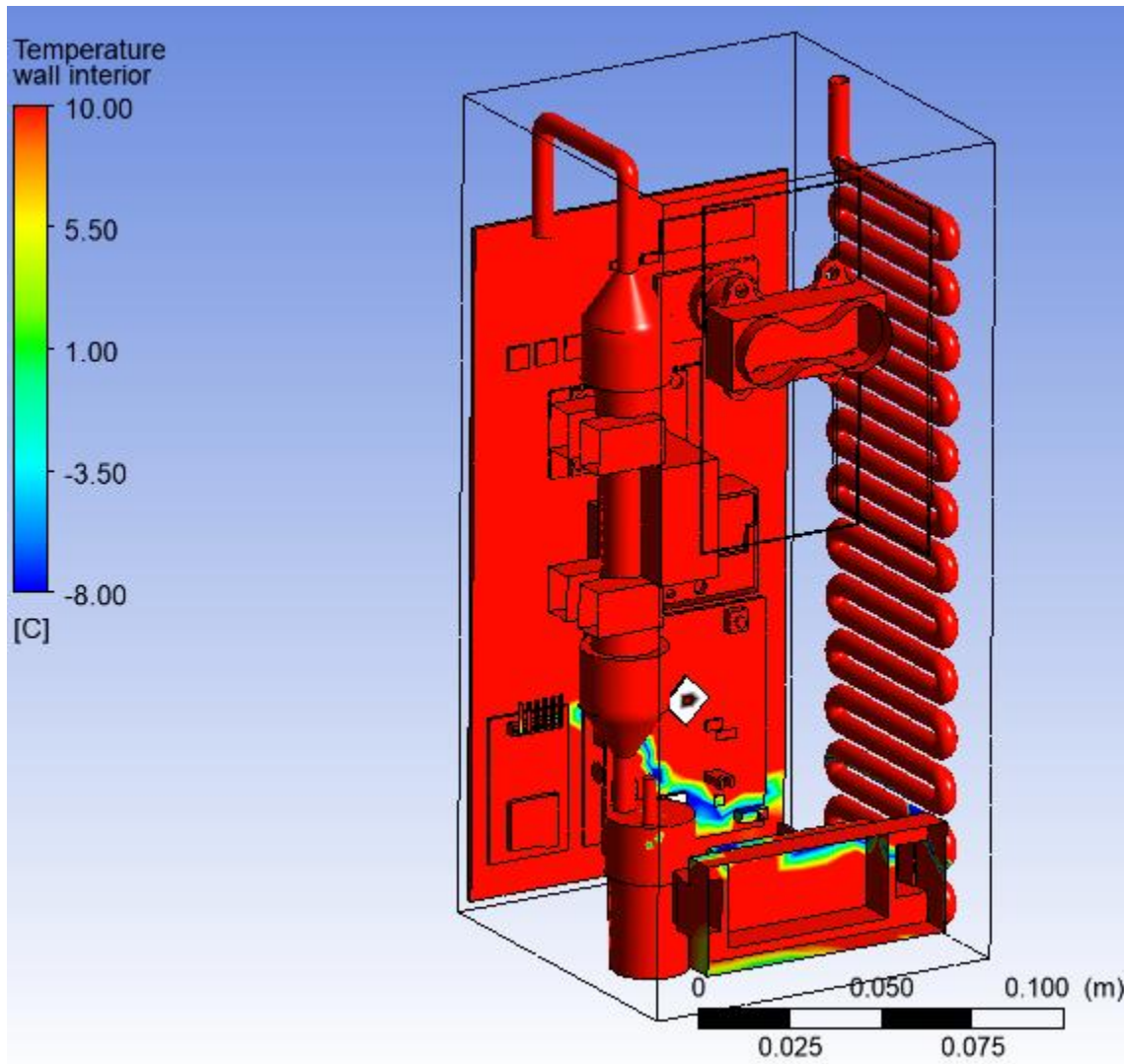


Fig. 37. Temperature distribution with heating pads.

2. Team Structure and Management

2.1 Team Organization and Roles

The WANKA project is led by Ramiro Tintaya as part of the activities of the research group of the same name. Ramiro Tintaya will be responsible for the management of the team's activities, as well as for the monthly reprimands. The project has the advice of Luis Suarez, from Geophysical Institute of Peru (IGP), who has experience in atmospheric physics. For a better distribution of tasks, the WANKA team has been divided into 5 teams. One team is in charge of programming and testing the Lidar, it is composed of Dario Huanca in charge of Lidar programming. Ramiro Tintaya, who will be in charge of Lidar data processing, and Germain Rosadio who will work on optics needed for the proper functioning of the LIDAR. Also, considering the conditions to which the payload will be exposed, a thermal and fluids simulation team was formed, led by Giusep Baca, who is working on the simulation of the external structure, as well as Jose Chong, who is working with the internal thermal flow simulations. Besides, Josue Huaroto will integrate the conduction heating system, and Jean Piere Cholán will support the development of the

simulations, in addition to structuring the organization of the group using frameworks as Scrum and applications as ClickUp that allow a better team organization management. The mechanical design team is led by Marco Chiroque, who studies the properties of the thermal insulation materials, Zedrix Quispe will simulate the structure with the mechanical loads, and Julver Marrufo will design the structure and distribute the components. There is also a team in charge of the microcontrollers programming led by Jose Robles who will be in charge of the active thermal control, Lucas Taipe will program the sensors that measure the critical parameters of the payload and Aníbal Esquiembre will work on the control of the airflow using the pump. Finally, the team in charge of the connections and power supply of the components is led by Miguel Morales who will be in charge of the energy distribution of the sensors and actuators, and David Arrustico who will design the PCB, they will also study the effects of the vacuum in the circuits and the adequate selection of electronic components considering the mentioned effects.

Table 4.1. Roles, names, institution, and contact information of the principal investigator and consultant.

Role	Name	Institution	Contact Information
Principal Investigator	Luis Fernando Suarez Salas	Instituto Geofísico del Perú Lima-Perú	lsuarez@igp.gob.pe +51 961-611-454
Microcontroller team consultant	Moises Stevend Meza Rodriguez	Universidad del Callao Lima-Perú	moises.meza@upch.pe +51 931-091-612

Table 4.2. Roles, names institution, and contact information of the student team.

Student Team Organization				
Role	Name	Academic Year	Institution	Contact Information
Project Manager	Ramiro Gustavo Tintaya Quispe	5	Universidad Nacional de Ingeniería Lima-Perú	rtintayaq@uni.pe +51 954-154-873
LIDAR team leader	Dario Adolfo Huanca Paredes	4	Pontificia Universidad Católica del Perú Lima-Perú	dario.huanca@pucp.edu.pe +51 957-742-086
LIDAR team member	Germain Rosadio Vega	4	Universidad Nacional de Ingeniería Lima-Perú	grosadiov@uni.pe +51 997-813-640
Simulations team leader	Giusep Alexander Baca Bernabe	5	Universidad Nacional de Ingeniería Lima-Perú	gbacab@uni.pe +51 997-218-987
Simulations team member	Jose Maria Chong Luna	5	Universidad Nacional de Ingeniería Lima-Perú	jose.chong.l@uni.pe +51 923-720-617
Simulations team member	Josue Santos Huaroto Villancencio	4	Universidad Nacional de Ingeniería Lima-Perú	josue.huaroto.v@uni.pe +51 953-254-024

Simulations team member	Jean Piere Cholán Llamoga	4	Universidad Nacional de Ingeniería Lima-Perú	jcholanl@uni.pe +51 947-167-058
Mechanic design team member	Marco Enmanuel Chiroque Espinoza	4	Universidad Nacional de Ingeniería Lima-Perú	mchiroquee@uni.pe +51 918-844-069
Mechanic design team member	Zedrix Augusto Quispe Carrillo	3	Universidad Nacional de Ingeniería Lima-Perú	zaquispec@uni.pe +51 965-069-548
Mechanic design team member	Julver Renaldo Marrufo Palli	4	Universidad Nacional de Ingeniería Lima-Perú	jmarrufop@uni.pe +51 917-315-573
Microcontroller team leader	Jose Andre Robles Loro	5	Universidad Nacional de Ingeniería Lima-Perú	jose.robles.l@uni.pe +51 924-869-359
Microcontroller team member	Anibal Esquiembre Quiros	3	Universidad Nacional de Ingeniería Lima-Perú	anibal.esquiembre.q@uni.pe +51 993-680-509
Power supply team leader	Miguel Morales Gonzales	5	Universidad Nacional de Ingeniería Lima-Perú	miguel.morales.g@uni.pe +51 924-482-219
Power supply team member	Lucas Nicolas Taipe Ramos	4	Universidad Nacional de Ingeniería Lima-Perú	ltaiper@uni.pe +51 920-594-837

Power supply team member	David Sergio Arrustico Villanueva	3	Universidad Nacional de Ingeniería Lima-Perú	david.arrustico.v@uni.pe +51 920-228-522
---------------------------------	-----------------------------------	---	--	---



Fig. 38. WANKA team members.

2.2 Timeline and Milestones

All the project activities are coordinated according to the SCRUM framework, this one allows us to react to unexpected changes, and ensure we obtain results in each iteration defined as a sprint, the ones that take place each two weeks. The first item in the Gantt diagram, WANKA Management, shows the milestones of the event and the organizational meetings where the tasks of each team are designated. Items 2, 3 and 4 specify the work organization of each team, previously designated in WANKA management. A reduced version of the Gantt diagram is shown in Fig. 39, and its detailed version is shown in the appendix.

December 2020

- 5 New members integration
- 12 General meeting /Designation of areas
- 19 Study of the phenomenon and mechanical simulations
- 26 Sprint Planning

January (01) 2021

- 2 Sprint Planning Resources
- 9 Application due
- 16 Component management
- 23 Sensor Programming and wiring/ Sprint Review January
- 30 Sensor testing and calibration/ sprint review January

February (02) 2021

- 6 Sensor testing/ Sprint Planning electronic
- 13 PCB printing and component soldering
- 20 Manufacture of the metal structure/ Sprint Review February
- 27 Rigid polyurethane foam layer implementation

March (03) 2021

6 Temperature/Vacuum tests/ Sprint Planning mechanic tests
13 Vacuum tests/ Sensor testing
20 Sprint Planning Application reviews
27 Sprint Review March & Teleconference

April (04) 2021

3 Electronic components integration/ Sprint Planning
10 Electronic tests
17 Draft PSIP/ Sprint Planning
24 Preliminary PSIP report/ Sprint retrospective & Review April &
Teleconference

May (05) 2021

8 Sprint Planning/possible structural fixes
15 Sensor calibration
22 Sprint Review May & Teleconference
29 Sprint retrospectives

June (06) 2021

5 Sprint Planning
12 Final Draft PSIP
19 Final PSIP/Sprint Review June & Teleconference
26 Sprint retrospectives

July (07) 2021

3 FLOP Draft 1
10 FLOP Final draft due
17 Final FLOP documents due
24 Sprint Review July & Teleconference

August (08) 2021

21 Sprint Review August & Teleconference
30 HASP Flight Preparation

September (09) 2021

04 Target Flight Ready/Target lunch date and flight
operation/Recovering, packing and return Shipping
18 Sprint Review September & Teleconference

October (10) 2021

23 Sprint Review October & Teleconference

November (11) 2021

20 Sprint Review November & Teleconference

December (12) 2021

01 Final Flight/Science Report Due

Table 5. Weight budget.

Component	Quantity	Mass (kg)	Method of measurement	Deviation +/-
Dust Sensor	1	0.025	According to vendor page [14]	Not specified
Gas Sensor	1	0.011	According to vendor page [15]	Not specified
Rotary Vane Pump	1	0.104	According to datasheet	Not specified
LIDAR	1	0.022	According to datasheet	Not specified
Flow Sensor AWM5101VN	1	0.060	According to datasheet	Not specified
Heating Pad 5x15 cm	1	0.005	According to SOLARIS 2018 Application	0.006
Temperature and relative humidity sensor	2	0.24	According to MOUSER ELECTRONICS [16].	Not specified
RTD Temperature Sensor	1	0.25	According to Alibaba [17].	Not specified
RTD Transmitter:	1	0.014	According to Amazon [18].	Not specified
GPS Module	1	0.009	According to Dualtronica [19].	Not specified
Pressure Sensor	1	0.02	According to Amazon [20].	Not specified
Current sensor	2	0.008	According to Amazon [21].	Not specified
Microcontroller	1	0.1	According to Amazon [22]	Not specified
Mechanical design				
Polyurethane foam lining	1	0.1278	According to mechanical simulation	Not specified

Hose circuit	1	0.026	According to mechanical simulation	Not specified
Aluminum 7075 structure	1	1.03	According to mechanical simulation	Not specified

3.2 Power Budget

Two PBY10 converters are connected to the 30V pins of the EDAC port through a 0.5A fuse to protect the payload. These converters will distribute the 15 watts that the HASP provides as it is shown in the preliminary drawings section (Fig. 40). The first PBY10 transmits 6W and the second 6.34 W, transmitting a total power of 12.34 W, which is the power consumed by the sensors and actuators. Power consumption of each component is explained in Table 6. LM1117 regulators will be used to supply 3.3V to the components that require this voltage. The only sensor that requires 10V is the flow sensor, this voltage is obtained using the +5v and -5v outputs of the second PBY10.

The system is protected using a fuse with these characteristics:

- Rated current (In.) 500 mA
- Maximum voltage drop 1 V
- Dimensions 5 × 20 mm

Table 6. Electronic components power budget.

Name (Quantity)	Current draw	Method of measurement	Uncertainty	Transient state	Steady state	Power consumption
Dust Sensor (1)	11 mA	According to Datasheet	Not specified	Not specified	Not specified	55mW
Gas Sensor (1)	150 mA	According to Datasheet	Not specified	Not specified	Not specified	750mW
Rotary vane pump (1)	285 mA	According to Datasheet	Not specified	Not specified	Not specified	1.425W
LIDAR (1)	135mA	According to Datasheet	Not specified	Not specified	Not specified	675mW
Heating Pad 5x15 cm (3)	600mA	According to Datasheet	Not specified	Not specified	Not specified	9W
Flow Sensor AWM5101VN (1)	10mA	According to Datasheet	Not specified	Not specified	Not specified	100mW

RS 232 Transceiver (1)	100mA	According to Datasheet	Not specified	Not specified	Not specified	1W
GPS NEO-6M (1)	37mA	According to Datasheet	Not specified	Not specified	Not specified	185mW
MAX31865 (1)	2mA	According to Datasheet	Not specified	Not specified	Not specified	6.6mW
RTD Pt100 (1)	2mA	According to Datasheet	Not specified	Not specified	Not specified	6.6mW
ACS712T (2)	12 mA	According to Datasheet	Not specified	Not specified	Not specified	120mW
SHT31(2)	1.5mA	According to Datasheet	Not specified	Not specified	Not specified	3mW
PRESSURE SENSOR (MS5611)	1.4mA	According to Datasheet	Not specified	Not specified	Not specified	4.62mW
MICRO-SD	40mA	According to Datasheet	Not specified	Not specified	Not specified	200mW
Microcontroller board (EK-TM4C123GXL)	303mA	Approximation according to Datasheet	Not specified	Not specified	Not specified	1W

3.3 Downlink Serial Data

As specified in the HASP Student Payload Interface Manual, our small payload will work with a baud rate of 1200. The serial link will be connected at 1200 baud rated using 8 data bits, no parity, and 1 stop bit as described in the manual.

As shown in Table 7, our Data Structure was formatted according to the suggested student data format. This package consists of various flight and systems monitoring data such as temperature, humidity, pressure on Lidar sensor and PCB Circuit as well as input current of the voltage converters. Additionally, we will be sending important data for the research project such as the aerosol concentrations and received signal strength obtained from the GP2Y1010AU0F and Lidar Lite V3 sensor respectively. Thus, considering that we will be sending a data stream of 36 bytes each minute, according to HASP documentation our bit rate is around 5 bps (bits per second) which is significantly below the upper limit of 1200bps and the maximum bps of the RS232 transceiver.

Table 7. Telemetry Package Data Structure.

Byte	Bits	Description
1	0-7	Record Type Indicator
2-5	0-31	Timestamp (seconds since January 1, 1970)
6-7	0-15	Record Size
8	0-7	Least Significant 8 bits of the record checksum
9-10	0-15	Temperature on Lidar Sensor
11-12	0-15	Humidity on Lidar Sensor
13-14	0-15	Pressure on Lidar Sensor
15-16	0-15	Temperature on PCB Circuit
17-18	0-15	Humidity on PCB Circuit
19-20	0-15	Pressure on PCB Circuit
21-24	0-31	Input Current PBY10
25-28	0-31	Input Current LM1117
29-32	0-31	Aerosol Concentrations GP2Y1010AU0F
33-36	0-31	Lidar Lite V3 Lectures

3.4 Uplink Serial Commanding

This mission does not require uplink serial commands.

3.5 Analog Downlink

This mission does not require analog downlink information either.

3.6 Discrete Commanding

This mission does not require discrete commands either.

3.7 Payload Location and Orientation Request

The payload must be oriented so that the lens of the lidar is facing away from the HASP platform as the lidar must be in contact with the circulating air. As the connection with the platform is symmetrical, there is no problem, only the above mentioned must be ensured.

There is no seat preference.

3.8 Special Requests

No special requests are needed for this mission.

4. Preliminary Drawings and Diagrams

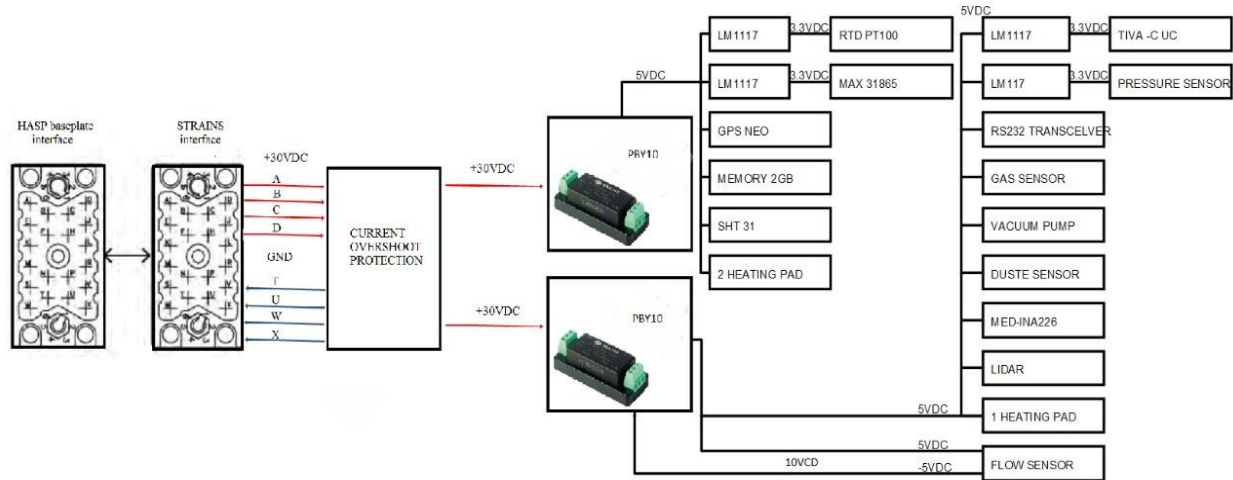


Fig. 40. Power Distribution Diagram.

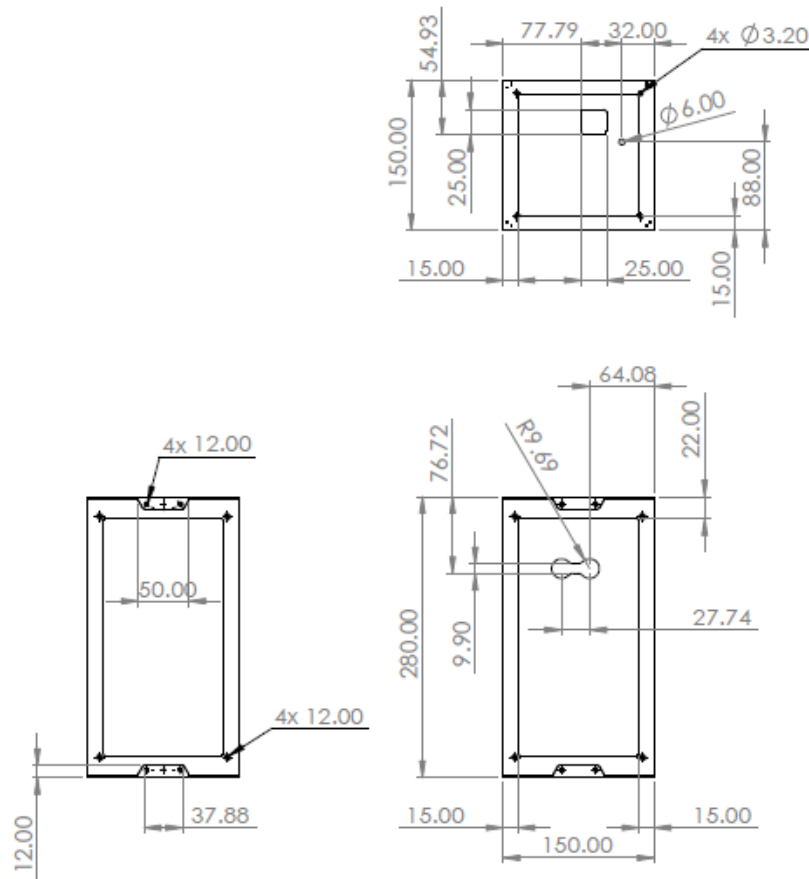


Fig. 41. Payload dimensions in millimeters.

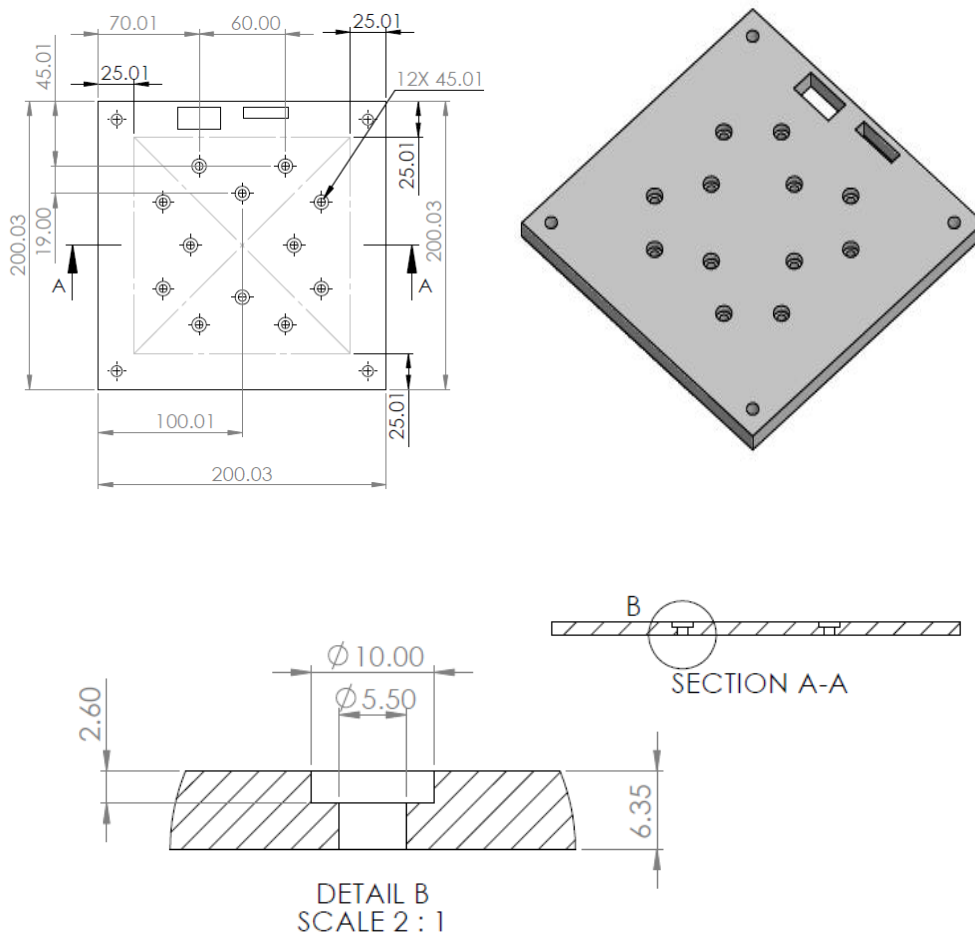


Fig. 42. Modification of the payload mounting plate with dimensions in millimeters.

5. References

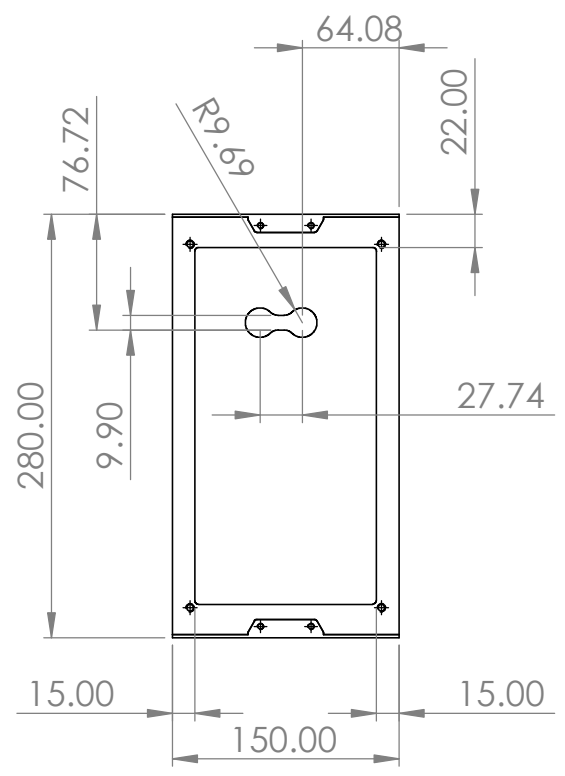
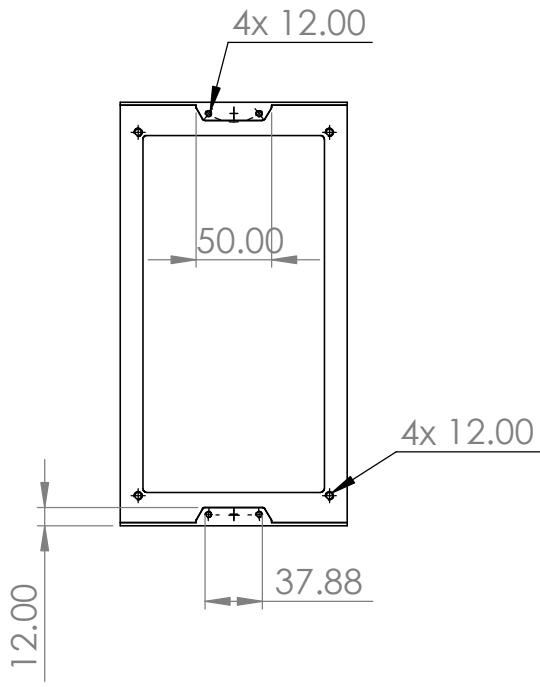
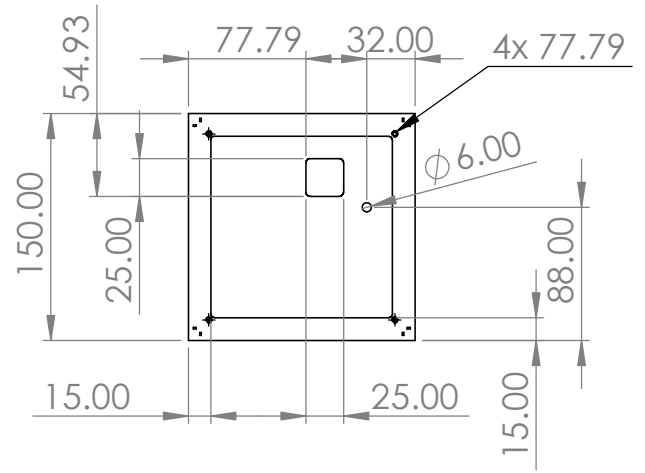
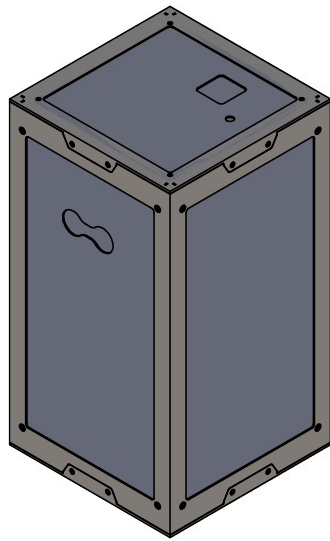
- [1] C. Timmreck, M. Toohey, A. Stenke, J. P. Schwarz, and R. Weigel, "Reviews of Geophysics and impact on climate," pp. 1–58, 2016, doi: 10.1002/2015RG000511.
- [2] J. Haywood and O. Boucher, "Estimates of the direct and indirect radiative forcing due to tropospheric aerosols: A review," *Rev. Geophys.*, vol. 38, no. 4, pp. 513–543, 2000, doi: 10.1029/1999RG000078.
- [3] J. Huang, B. Mendoza, J. S. Daniel, C. J. Nielsen, L. Rotstayn, and O. Wild, "Anthropogenic and natural radiative forcing," *Clim. Chang. 2013 Phys. Sci. Basis Work. Gr. I Contrib. to Fifth Assess. Rep. Intergov. Panel Clim. Chang.*, vol. 9781107057999, pp. 659–740, 2013, doi: 10.1017/CBO9781107415324.018.
- [4] T. N. Knepp *et al.*, "Evaluation of a method for converting Stratospheric Aerosol and Gas Experiment (SAGE) extinction coefficients to backscatter coefficients for intercomparison with lidar observations," *Atmos. Meas. Tech.*, vol. 13, no. 8, pp. 4261–4276, 2020, doi: 10.5194/amt-13-4261-2020.
- [5] S. Brunamonti *et al.*, "Validation of aerosol backscatter profiles from Raman lidar and ceilometer using balloon-borne measurements," *Atmos. Chem. Phys. Discuss.*, no. May, pp. 1–31, 2020, doi: 10.5194/acp-2020-294.

- [6] S. Kotthaus *et al.*, “Recommendations for processing atmospheric attenuated backscatter profiles from Vaisala CL31 ceilometers,” *Atmos. Meas. Tech.*, vol. 9, no. 8, pp. 3769–3791, 2016, doi: 10.5194/amt-9-3769-2016.
- [7] J. M. Rosen and N. T. Kjome, “Backscattersonde: a new instrument for atmospheric aerosol research,” *Appl. Opt.*, vol. 30, no. 12, p. 1552, 1991, doi: 10.1364/ao.30.001552.
- [8] M. Petersen, B. Stephens, J. E. Sohl and F. Brown “A Balloon-Borne Optical System for Measuring In-Situ PM2.5 Aerosol Concentrations,”
- [9] T. T. Sekiyama, T. Y. Tanaka, A. Shimizu, and T. Miyoshi, “Data assimilation of CALIPSO aerosol observations,” *Atmos. Chem. Phys.*, vol. 10, no. 1, pp. 39–49, 2010, doi: 10.5194/acp-10-39-2010.
- [10] A. Comerón, C. Muñoz-Porcar, F. Rocadenbosch, A. Rodríguez-Gómez, and M. Sicard, “Current research in lidar technology used for the remote sensing of atmospheric aerosols,” *Sensors (Switzerland)*, vol. 17, no. 6, pp. 1–16, 2017, doi: 10.3390/s17061450.
- [11] D. Fappani and P. Robert, “Cryogenic optics for space application,” vol. 10563, no. October 2014, p. 116, 2017, doi: 10.1117/12.2304176.
- [12] Lidar Live v3 Operation Manual and Technical Specifications, Garmin Ltd., New Taipei City, Taiwan, 2016.
- [13] Precup, R., Radac, M., Roman, R., & Petriu, E. M. (2017). Model-free sliding mode control of nonlinear systems: Algorithms and experiments. *Information Sciences*, 381, 176-192. doi: 10.1016/j.ins.2016.11.026.
- [14] “GP2Y1010AU0F Compact Optical Dust Sensor,” iteadstudio. [Online]. Available: <https://www.itead.cc/gp2y1010au0f-compact-optical-dust-sensor.html>.
- [15] ePro Labs MQ-135 Air Quality Gas Sensor Module: Amazon.in: Industrial & Scientific. [Online]. Available: <https://www.amazon.in/ePro-MQ-135-Quality-Sensor-Module/dp/B00D04LB2O>.
- [16] “SHT31-ARP-B2.5kS Sensirion: Mouser,” *Mouser Electronics*. [Online]. Available: https://www.mouser.pe/ProductDetail/Sensirion/SHT31-ARP-B25kS/?qs=/ha2pyFadugVO99f9g9Mhf0P/23UOnc04DATsGm5V69MFKCIFn9Abw==_
- [17] “2m De Acero Inoxidable De Idt Pt100 Sensor De Temperatura Sonda Térmica Termopar Detector Comprobador De M8 Hilo Industrial De Sensor - Buy Pt100 Sonda Termopar Pt100 Termopar Pt100 Sensor De Temperatura Product on Alibaba.com,” *www.alibaba.com*. [Online]. Available: https://spanish.alibaba.com/product-detail/2M-Stainless-Steel-RTD-PT100-Temperature-60868332875.html?mark=shopping&src=sem_ggl&cmpgn=11760085347&adgrp=117132382271&locintrst=&locphyscl=9060924&ntwrk=u&device=c&dvcmdl=&position=&pla_adtype=&pla_mrctid=254528571&pla_channel=online&pla_prdid=60868332875&pla_country=PE&pla_lang=es&pla_group=293946777986&pla_localcode=&gclid=Cj0KCQiA3NX_BRDQARIsALA3fILvjS-jWWKCNrym8dWoyN1kHvwCXF5Myq6xQYIjsCpiSa1PDvpSX2caAmrhEALw_wcB#shopping-ads.

- [18] “Comidox MAX31865 PT100/PT1000 RTD - Sensor de temperatura para Arduino,” *Amazon.com: Electrónica*. [Online]. Available: <https://www.amazon.com/-/es/Comidox-MAX31865-PT100-PT1000-RTD/dp/B07PDFNZYX>.
- [19] “GPS ARDUINO NEO-6M,” *Dualtronica*. [Online]. Available: <https://dualtronica.com/modulos/86-modulo-gps-neo-6m.html>.
- [20] “ARCELI GY-63 Precision MS5611-01BA03 - Módulo de sensor de presión atmosférica,” *Amazon.com: Electrónica*. [Online]. Available: https://www.amazon.com/-/es/ARCELI-GY-63-Precision-MS5611-01BA03-atmosf%C3%A9rica/dp/B07DN2H2FR/ref=pd_sbs_21_7?_encoding=UTF8&pd_rd_i=B07DN2H2FR&pd_rd_r=249d3f73-9ed5-4f21-adbf-71d29ce4bde9&pd_rd_w=iIDCR&pd_rd_wg=KYEM6&pf_rd_p=3ec6a47e-bf65-49f8-80f7-0d7c7c7ce2ca&pf_rd_r=S9BE99B2TR2VART2P3ZT&psc=1&refRID=S9BE99B2TR2VART2P3ZT#descriptionAndDetails.
- [21] “SMAKN 2pcs ACS712T IIC I2C Interface Bi-Directional Current Sensor,” *Amazon.es: Electrónica*. [Online]. Available: <https://www.amazon.com/-/es/TRTV1648/dp/B00FIKRXRK>.
- [22] “Placas y juegos de desarrollo - ARM TIVA Launchpad,” *Amazon.es: Electrónica*. [Online]. Available: <https://www.amazon.com/Development-Boards-Kits-TIVA-LaunchPAD/dp/B00HKIDHI2>

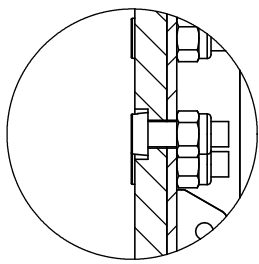
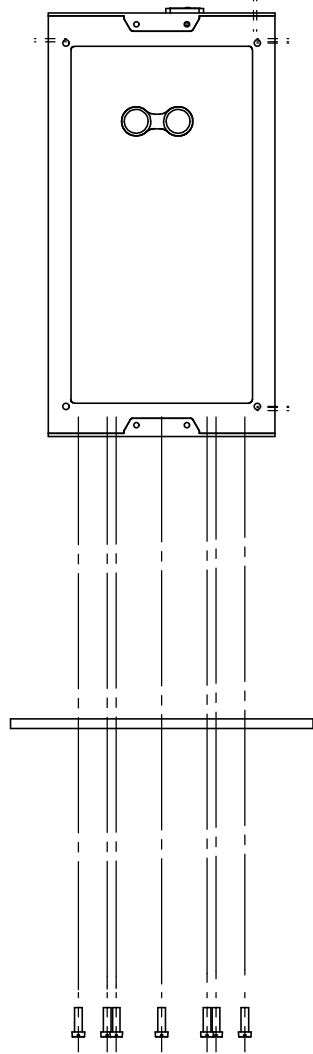
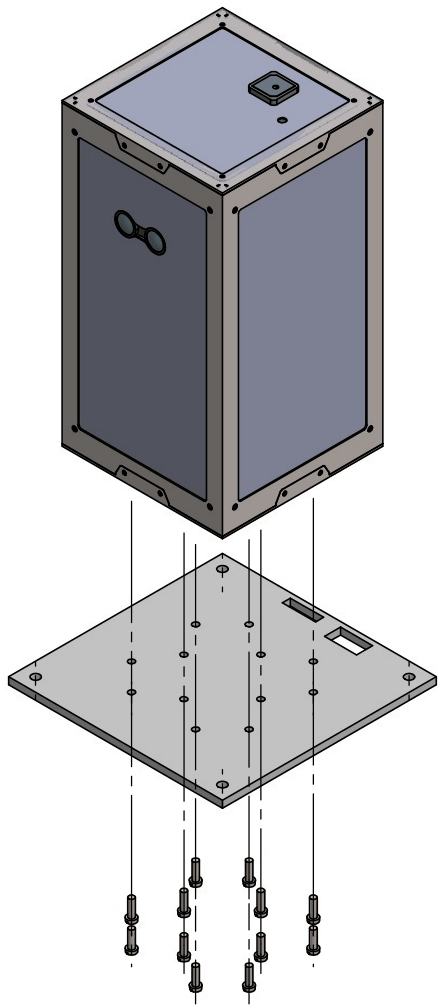
Appendix

Detailed mechanical drawings not required in previous sections

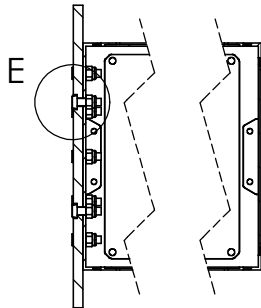


TITLE:				PAYLOAD DIMENSIONS	
MATERIAL:		FILENAME:		DGPN01	
Aluminio 7075					
MASS:		SCALE:		UNITS:	
1.03 Kg		1:5		mm	
				SHEET 1 OF 1	

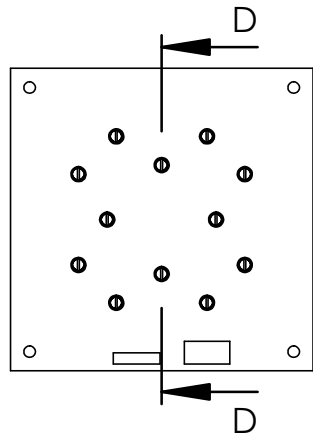
A4



DETAIL E
SCALE 2 : 3



SECTION D-D



TITLE:
PAYLOAD MOUNTAING PLATE
INTERFACE

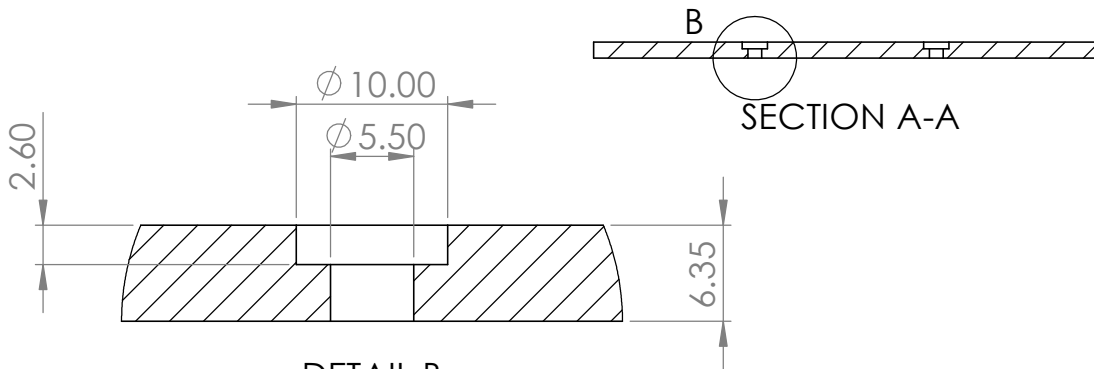
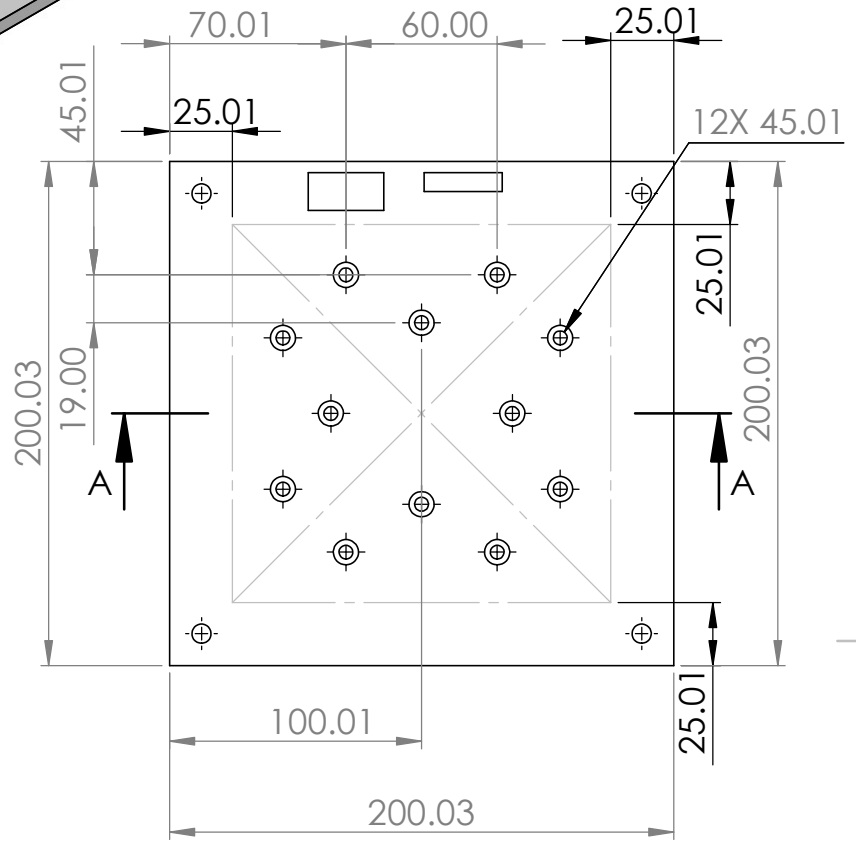
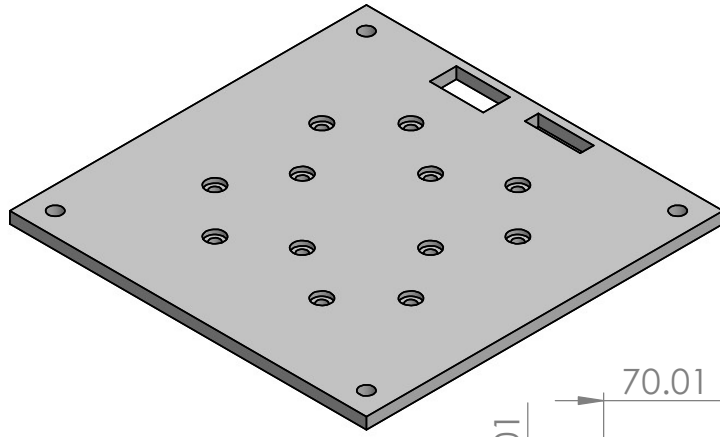
FILENAME:

DPMP01

A4

SCALE:1:5

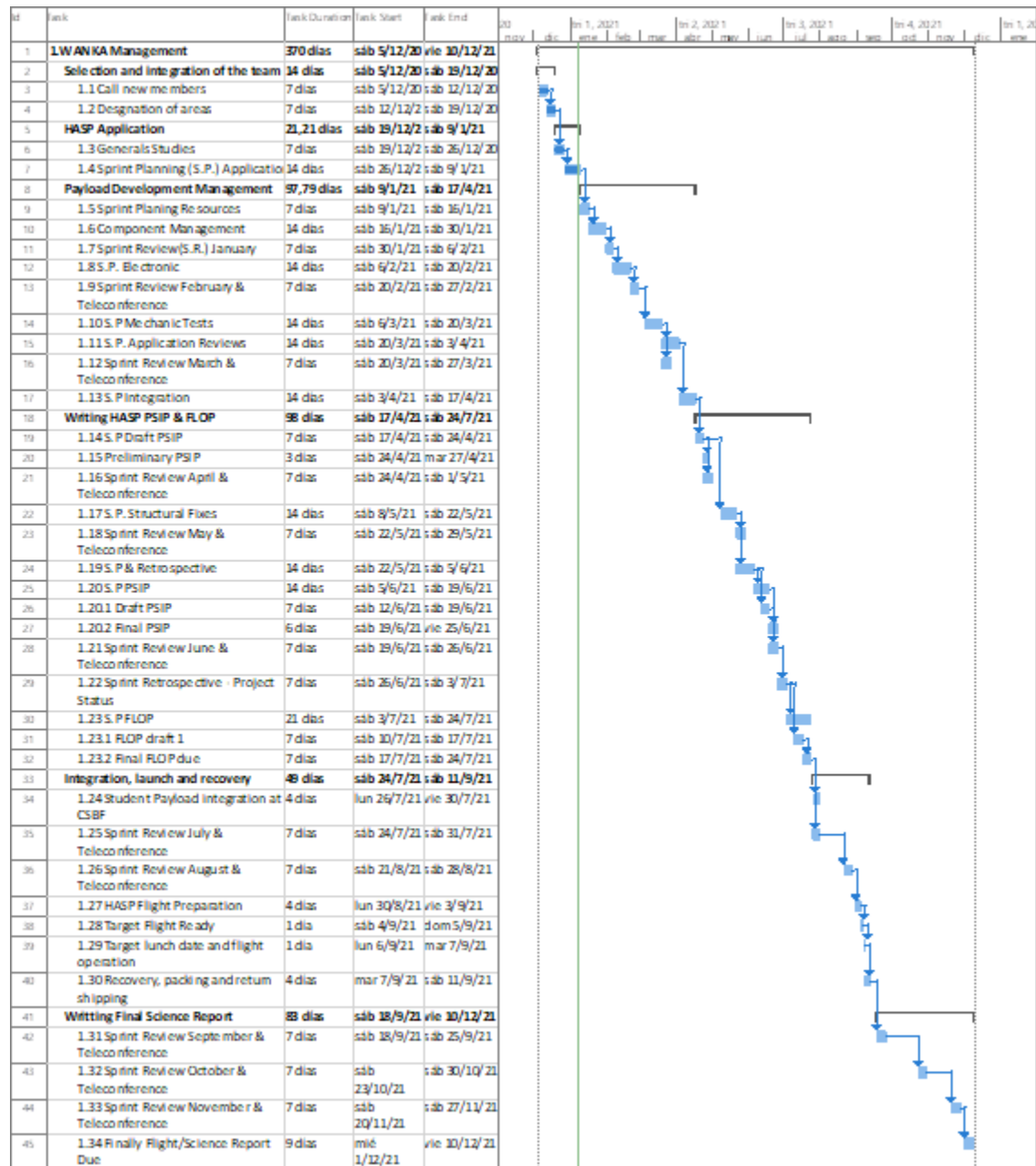
SHEET 1 OF 1



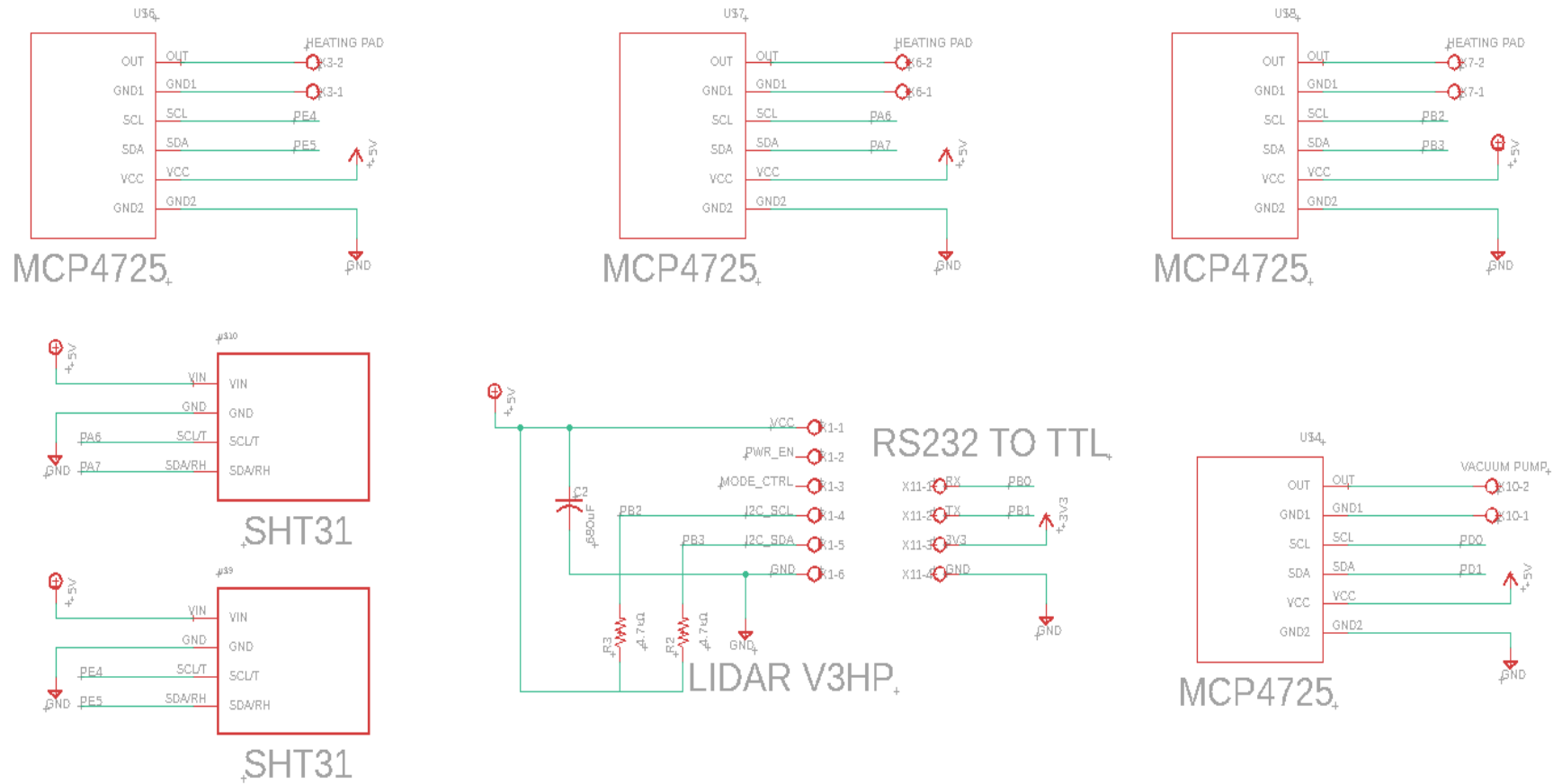
DETAIL B
SCALE 2 : 1

TITLE: MODIFIED PAYLOAD MOUNTING PLATE		
MATERIAL: PVC	FILENAME: DMPI02	A4
UNITS: mm	SCALE:1:3	SHEET 1 OF 1

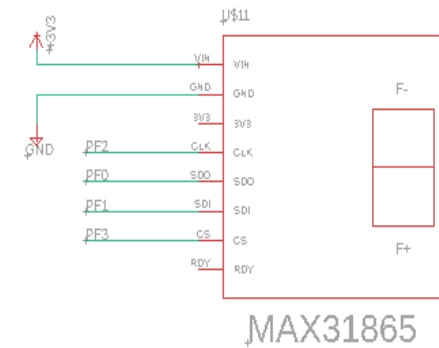
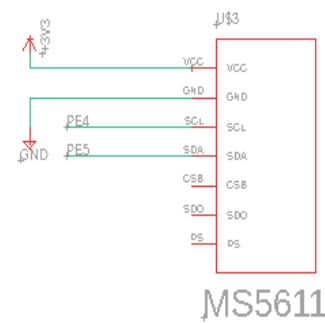
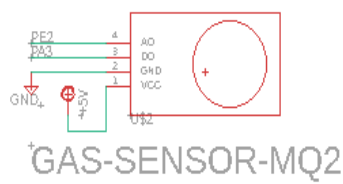
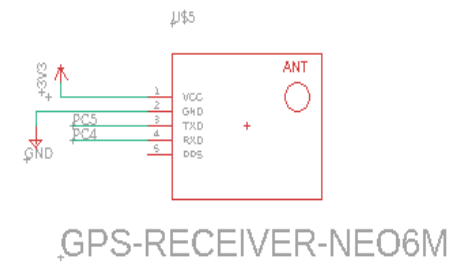
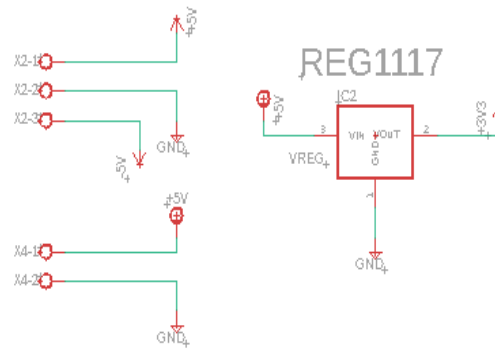
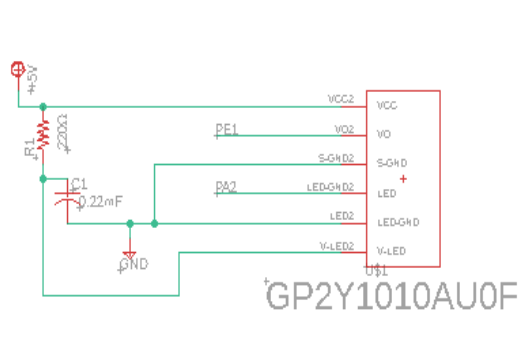
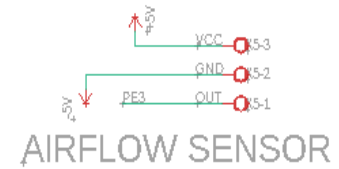
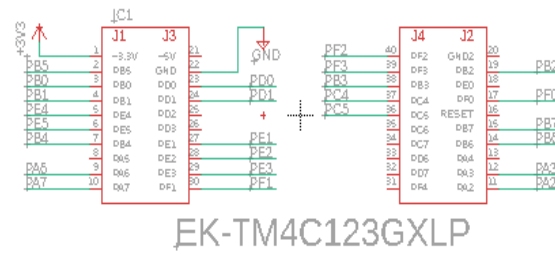
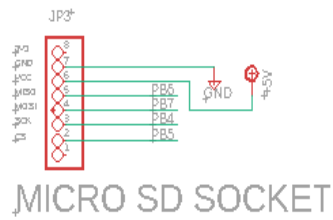
Detailed timeline and milestone WBS document



Detailed electrical drawings not required in previous sections

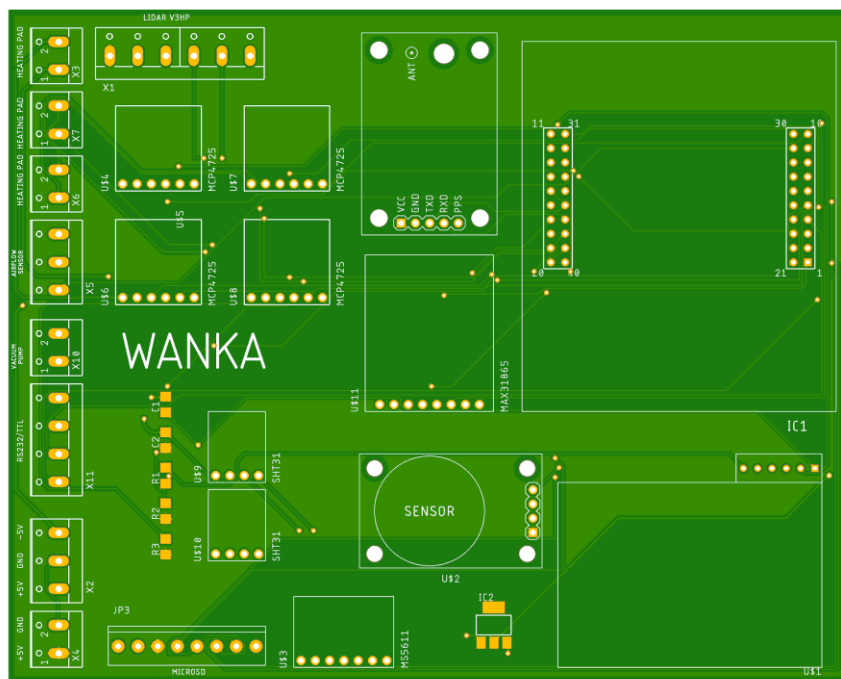
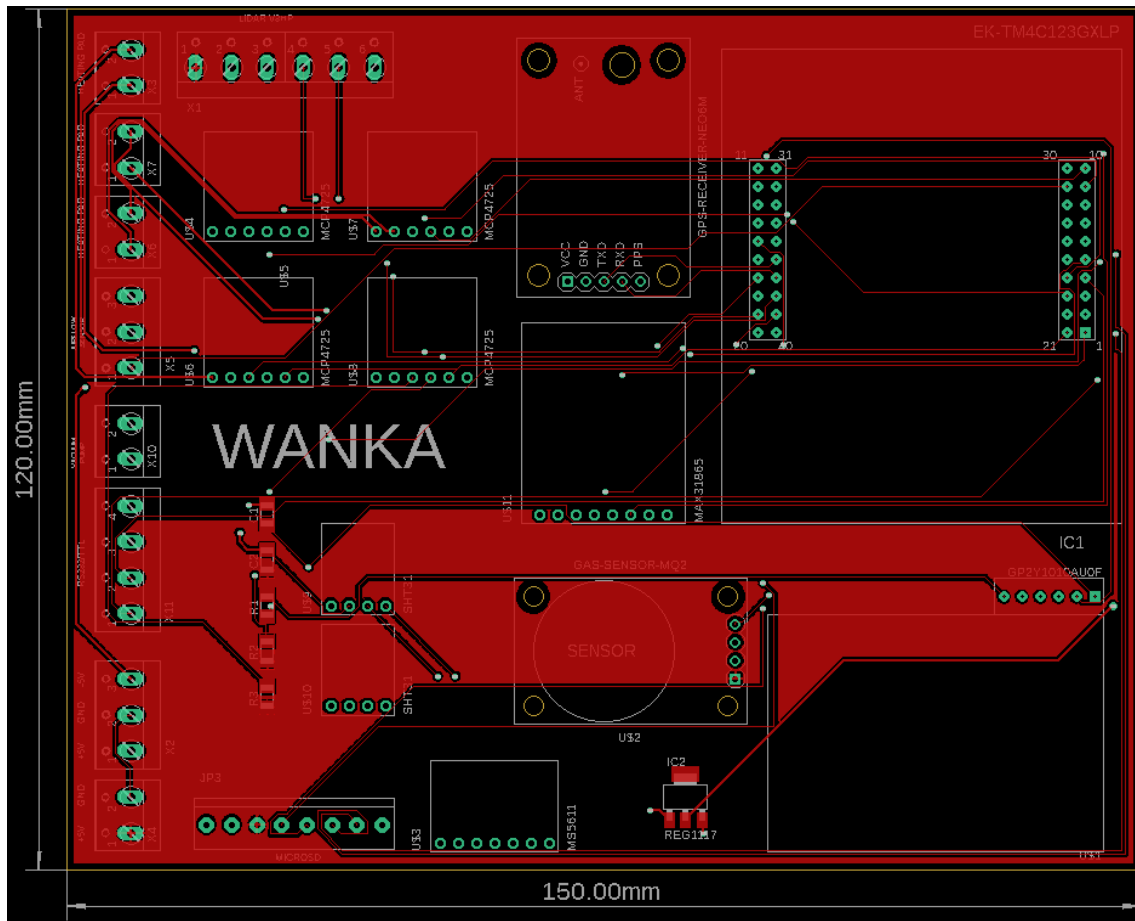


First half of the schematic design

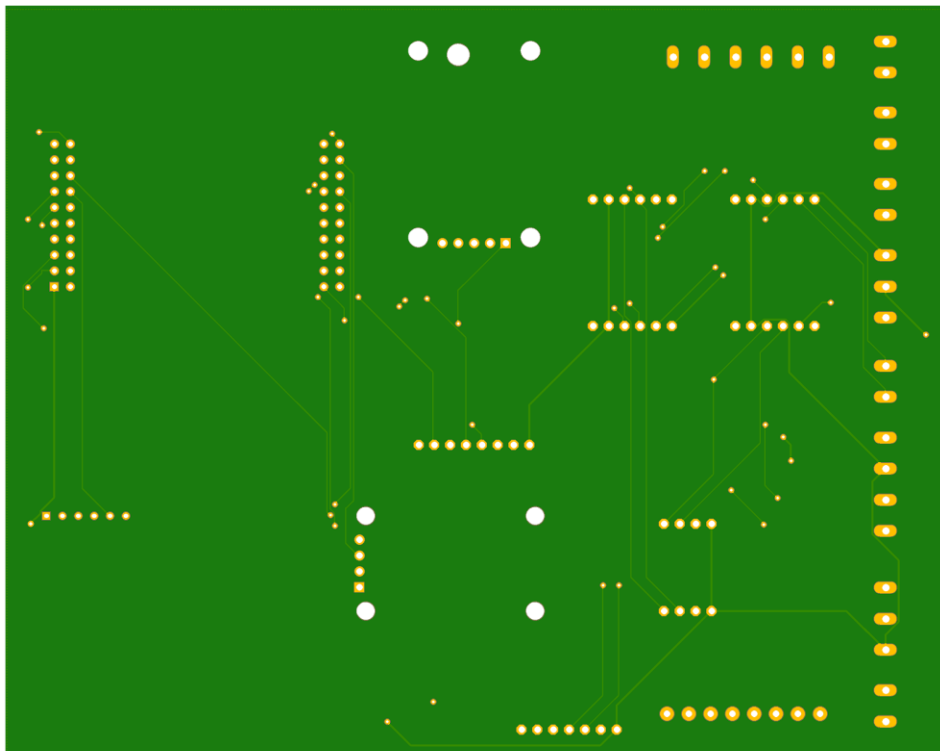
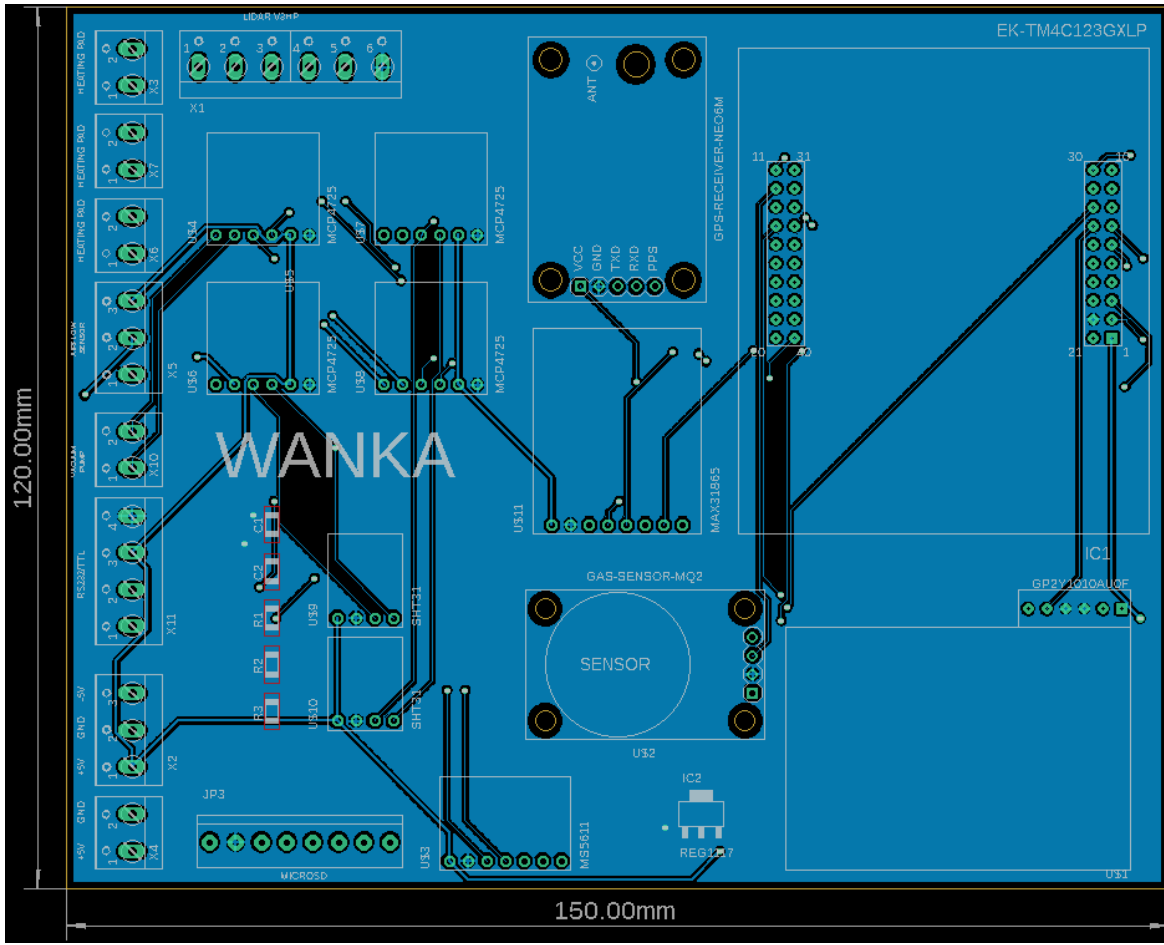


Second half of the schematic design

Preliminary PCB layout



Top side views



Bottom side views